Detecting sensitive areas in confined shallow basins

Detecting sensitive areas in confined shallow basins

Francesca De Serio[1,2,*], Elvira Armenio[3], Mouldi Ben Meftah[1,2], Gennaro Capasso[4], Vera Corbelli[4], Diana De Padova[1,2], Francesca De Pascalis[5], Annalisa Di Bernardino[6], Giovanni Leuzzi[7], Paolo Monti[7], Agnese Pini[7], Raffaele Velardo[4], Michele Mossa[1,2]

[1] Polytechnic University of Bari, DICATECh, Bari, Italy

[2] CoNISMa, Inter University Consortium for Marine Sciences, Rome, Italy

[3] Brindisi Municipality, Brindisi, Italy

[4] Southern Hydrological Authority, Caserta, Italy

[5] Institute of Marine Sciences, ISMAR, Venezia, Italy

[6] University Roma La Sapienza, Physics Department, Roma, Italy

[7] University Roma La Sapienza, DICEA, Roma, Italy

* Corresponding author: francesca.deserio@poliba.it

Highlights

- Meteorological and hydrodynamic models to investigate physical processes in a coastal basin
- Field measurements calibrating numerical models
- Indicators selected to identify sensitive areas in the basin

Abstract

Coastal shallow basins are often heavily anthropized and greatly exposed to environmental risk areas, thus requiring strict monitoring action by local authorities and stakeholders. Preventive measures against environmental degradation and early warning to hazards have been proved to benefit from the combined use of numerical models and field measurements. The present work sets out to show the potential of a meteorological-hydrodynamic model system, validated with field data, to identify the main physical processes characterizing a semi-enclosed basin located in the inner part of the Ionian Sea, in southern Italy. Furthermore, based on the model results, we adopted some convenient indicators, especially related to flow exchanges, in order to identify and characterize the area in the basin most sensitive to environmental problems. The results highlight the retentive feature of the inner part of the basin and different times necessary for the water renewal in both the surface and bottom layers.

Keywords: field measurements, meteorological model, hydrodynamic model, semi-enclosed basin, sea currents.

1. INTRODUCTION

A common challenge in coastal management is to balance environmental conservation priorities, human activities and economic development. An essential tool in the decision support system is the possibility to detect and identify the most sensitive coastal areas, i.e. areas exposed to strong human and industrial pressure, where environmental problems, especially linked to transport and diffusion of pollutants, assume relevant importance. There are many pollutant sources in heavily anthropized coastal sites; unfortunately, available data to identify them and to establish their greater or lesser danger are often scarce. Widespread pollutant inputs can even be associated with inland sources and can be transported underground in the aquifer and discharged into the sea. Consequently, knowledge of possible paths and fate of polluting tracers, sediments trapping, water renewal times is of paramount importance for coastal management plans and in situ decision-making. Moreover, the mapping of the most critical and sensitive areas within a coastal basin, based on some key factors, could be of great benefit for this scope, guiding possible monitoring actions and rehabilitation interventions (Armenio et al., 2018; 2019; De Serio and Mossa, 2016; De Serio and Mossa, 2018; De Padova et al., 2017; De Carolis et al., 2013; Kjerfve and Magill, 1989). This is the main reason for the present study.

Nowadays, predictive operational oceanography takes into account regional, sub-regional and shelf-coastal scales, based on coupled models of wave, current and tracer dynamics. The interaction between sea and atmosphere is often limitedly modeled by means of empirical bulk formulas, providing wind stress as a function of wind velocity and depending on empirical drag coefficients (Samaras et al., 2016; Gaeta et al. 2016; Wróbel-Niedźwiecka et al., 2019). This approach must face some limitations to provide reliable results on the sea circulation in the basin. In fact, understanding the physical processes involved at the atmosphere-sea interface is complex as well as essential, especially in terms of exchange of momentum between wind and sea surface (Di Bernardino et al., 2016). Thus, it is desirable to address numerical meteorological models simulating the overlying atmospheric flow. In this way, meteorological input data, such as wind speed and direction, air temperature and atmospheric pressure, among others, can be used as boundary conditions at the atmosphere-sea interface. Furthermore, hydrodynamic numerical models need a setup, a calibration and a validation, so that their integration with waves, current and tide data is fundamental (Umgiesser et al., 2004; Armenio et al., 2016a; 2017; Cannata et al. 2018). It is also worth noting that the accuracy of model outputs relies on the quantity, quality and duration of the available observations. Therefore, extensive field measurements are of primary importance and monitoring actions should be judiciously programmed (Samaras et al., 2016; Trotta et al., 2017).

In this study, we aim to examine the main hydrodynamic processes in a coastal basin with lagoon features, which is assumed as a target case, by using a meteorological and a hydrodynamic model. A semi-enclosed basin located in southern Italy, exposed to heavy urban, industrial and military activities, was used for this scope (De Padova et al., 2017). The effectiveness of the proposed model chain was provided by comparing the model results and the field data, which were acquired onsite by means of two fixed monitoring stations and operational surveys. The runs covered an annual period and the model results were provided onto a mesh with

a high spatial resolution. In this way, we could identify some typical trends in the water circulation and exchanges, which makes it possible to detect the most vulnerable locations in the domain examined, based on some suitable indicators. Following Cucco and Umgiesser (2015) and De Pascalis et al. (2016a), the water transit time, the water renewal time and the trapping index were defined and computed for this scope.

The added value of this study with respect to previous numerical works applied to the same area (De Pascalis et al., 2016a,b) is in: i) the adoption of a meteorological model to provide time-varying and space-varying meteorological data, as realistic input for the implementation of the hydrodynamic model; ii) the time period used for the simulation, that is the whole year 2014 (while previous simulations referred to 2013), for which proper field measurements were available; iii) the computation of all the three indicators related to the basin vulnerability; iv) this computation was based on the entire annual period, rather than on a short time window (such as couple of months), thus resulting more reliable.

The paper is structured in the following way. Sections 2 and 3 respectively describe the area studied and the monitoring activity. Section 4 presents the numerical models used. Section 5 describes the validation of the model outputs with field data and the main hydrodynamic features. Section 6 identifies the key indicators used to assess the basin vulnerability. The discussion on these findings is in Section 7.

2. STUDY AREA

The proposed approach was applied to a target area located in the inner part of the Gulf of Taranto in the Ionian Sea, along the coast of Southern Italy (Fig. 1). The study area is composed of the Mar Grande and the inner basin of Mar Piccolo, which in turn consists of two bays, respectively named Bay I and Bay II. The Mar Grande and Mar Piccolo basins are joined by means of an artificial channel, namely the Navigable Channel (58m wide and 12m deep), and a natural one, namely the Porta Napoli Channel (150 m wide and 2.5 m deep). The total area of the Mar Piccolo is about 21.7 km^2 and the average depth is about 7 m. The total area of the Mar Grande is about 35 km^2, while its maximum depth is about 35 m in its central area. Along the outer perimeter of the Mar Grande there are two small islands, called Cheradi Isles, joined by a long breakwater. In the Mar Piccolo there are about 34 freshwater submarine sources of karst origin, called *citri* (Lisco et al., 2016). They can be temporary or permanent during the year, depending on the rainfall and the dynamics of the submarine water intrusion in the springs. The presence of these freshwater inputs influences the salinity gradients of the basin giving it the typical characteristics of a transitional environment (Umgiesser et al., 2014; De Pascalis et al. 2016b). In addition, a submarine freshwater source called citro San Cataldo, with an average flow rate of 2 m^3/s, is present at the mouth of the Porta Napoli Channel (Cardellicchio et al., 2013).

The environmental problems of this domain are related to the degraded conditions of the air, soil, water, sediments and biota environmental matrices. The basins represent ecosystems potentially influenced by different anthropogenic pressures: urbanization, industrial waste, agriculture, commercial fishing, and aquaculture. In particular, the basins include one of the most important steel production plants in Europe (ILVA), an oil refinery, a cement plant, two thermoelectric power plants, and three waste incinerators. In addition, the city of Taranto hosts an important commercial port and the main naval base of the Italian Navy,

located in Bay I of the Mar Piccolo and in the southern area of the Mar Grande. As a result, both basins are affected by pollutant loads due to numerous outflows from civil, military and industrial origins, which are authorized and monitored only in some cases. In the Mar Grande, these discharges are found mainly along its northern and northeastern coasts. On the other hand, superficial hydrography in the Mar Piccolo is extremely scarce due to the nature of the rocks and the subtropical climate. Furthermore, the Mar Piccolo has hosted several human activities for a long time and is home to the largest mussel farm in Italy which covers 65% of the total surface of both the bays, with a mussel production estimated to be approximately 64,000 t/year (Cardellicchio et al., 2016) (Fig. 1). The need for an assessment of models able to predict hydrodynamics and pollutant dispersion in the two water basins is imperative. This is further enhanced by the presence of two main rivers, which provide a limited contribution to the water inflow, i.e., the Galeso (~0.8 m^3/s) and the Canale D'Aiedda (~1 m^3/s) rivers, where the latter also carries wastewater from sewage plants (De Pascalis et al. 2016b).

3. MONITORING ACTIVITY

3.1. Fixed monitoring stations

In December 2013, a meteo-oceanographic station (Station O) was installed in the Mar Grande basin, at the geographical coordinates 40°27.6' N and 17°12.9' E (Fig. 1). The local depth in this station is on average equal to 23.5m. The station is provided with many instruments, including a bottom mounted Acoustic Doppler Current Profile (ADCP), a multidirectional wave array, a weather station and a CTD (measuring water salinity, water temperature and depth). In detail, the weather system combines an ultrasonic wind speed and direction sensor (accuracy ±2% and ±3° for velocity and direction, respectively) providing hourly averaged values. Velocity and direction of sea currents are measured by means of the ADCP, using a Janus configuration, which samples them along the water column with 0.50m vertical bin resolution and a 1.60m blanking distance. Mean current velocity profiles are collected continuously at hourly intervals, using an average of 60 measurements acquired every 10s. In this way, hourly averaged velocity components along the water column are available for analysis. In May 2014, a second monitoring station (Station N) was installed in the Navigable Channel (Fig. 1), equipped with a second bottom mounted ADCP and a wave array, also completed with the deployment of an ultrasonic tide gauge. It is located at the geographical coordinates 40.473° N and 17.235° E (Fig. 1). The local depth in this station is on average 13.7m. Also in this case, taking into account the ADCP size and its blanking distance, the current velocities are assessed along the vertical from the seabed, at constant intervals equally spaced every 0.5m. The acoustic frequency of both the ADCPs is 600KHz and their velocity accuracy is 0.3% of the water velocity. More details on the stations can be found in Armenio et al. (2016b) and De Serio and Mossa (2018).
The analysis presented in this study is based on the data collected in the target area including wind, waves and currents from January 2014 to December 2014 for Station O and from June 2014 to December 2014 for Station N. In particular, data recorded by Station O were used as input in the modelling phase (as described in Sect. 4.2.1), while data recorded by Station N were used to validate the hydrodynamic model (sect. 4.2.2).

3.2. *Ad hoc* monitoring surveys

The Institute of Marine Sciences of Venice of the National Research Council (CNR-ISMAR) and the DICATECh of the Polytechnic University of Bari carried out a measurement field campaign on November 26-27, 2014. During this campaign, data of water current, temperature and salinity were measured in the Mar Piccolo. The three velocity components of the sea current were acquired by means of a Vessel-Mounted Acoustic Doppler Current Profiler (VM-ADCP), while CTDs were used to record water temperature and salinity. Figure 2 shows the locations of the measurement standing stations. Current velocities and directions were assessed in six stationing points (BS) along the vertical, equally spaced every 0.50 m. Five of them are located in Bay I of the Mar Piccolo and one in Bay II (Table 1).

Figure 1. Target area and location of the fixed monitoring stations. Mussel farms limited by dotted lines. Google Earth source.

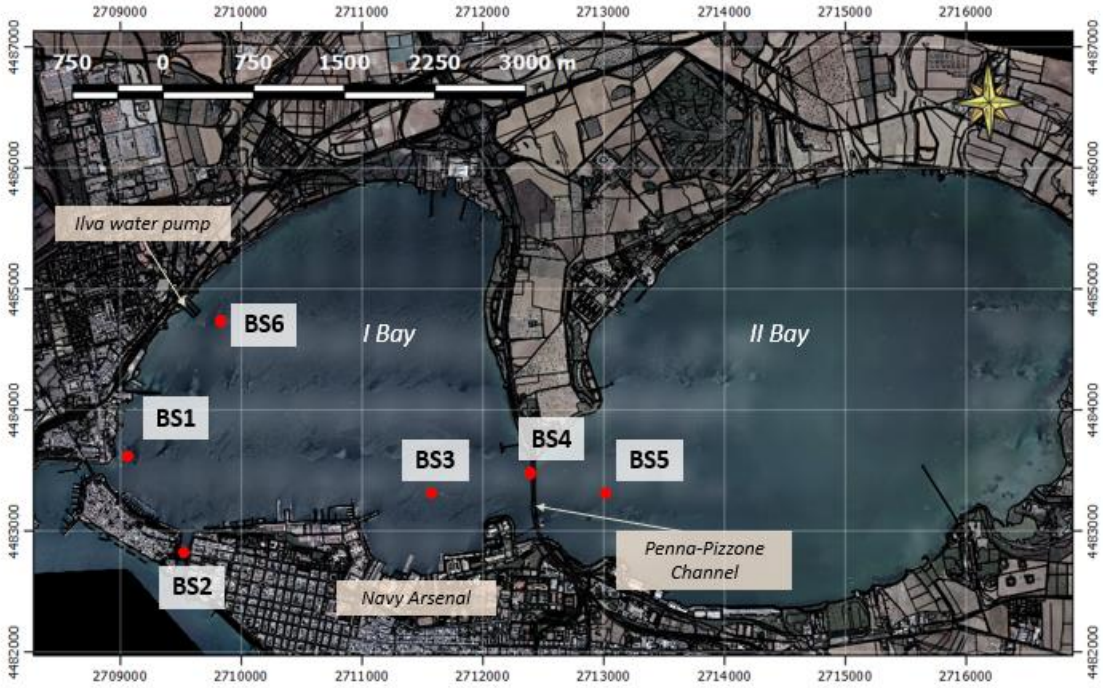

Figure 2: Location of measurement stations monitored during the campaign of November 26-27, 2014.

Table 1. Coordinates and position of BSs measuring stations

Base Station	Position	Gauss-Boaga Coordinates		Spatial location
		North	East	
BS1	Bay I	4483213.29	2709393.73	Old town
BS2	Bay I	4482749.67	2709557.61	Navigable Channel
BS3	Bay I	4483018.7	2711497.5	Navy Arsenal
BS4	Bay I-II	4483255.37	2712419.16	Penna-Pizzone Channel
BS5	Bay II	4483191.42	2713081.9	New Navy Arsenal
BS6	Bay I	4484699.36	2710045.58	ILVA waterpump

4. NUMERICAL MODELS

Based on the field data available, both models run to simulate the behavior of the two basins during the year 2014. First, the meteorological model was used to estimate the atmospheric flow in the area during the whole year. Then, these data were used as boundary conditions at the sea surface to force the hydrodynamic model together with other input data supplied by various national agencies in charge of monitoring them, as will be specified in the following. The results in terms of water velocity, temperature and salinity, were then compared with the field data to i) validate the models examined, ii) assess the water circulation pattern in the domain and iii) detect the associated temporal scales.

4.1 Meteorological model

The meteorological simulations were performed using the CALMET model (Scire et al., 2000). It is a mass-consistent, diagnostic meteorological model developed by the California Air Resource Board and successively improved by the U.S. Environmental Protection Agency. CALMET allows the reconstruction of the three-dimensional wind and air-temperature fields as well as the two-dimensional gridded fields of the main turbulence parameters, such as the Pasquill-Gifford stability classes, the Obukhov length and the mixing height.

In the present work, CALMET was used for the numerical simulation of the wind field in the study area and in particular to calculate the shear stress at the atmosphere-sea interface. It is worth noting that, in simple applications and for small domains, the value of the tangential stress inferred from wind measurements carried out in one point can be assigned as boundary condition on the entire sea surface. When referring to wider coastal domains, global forecasts and specific datasets provided by the European Centre for Medium-Range Weather Forecasts (ECMWF) are generally used to force the hydrodynamics, nevertheless they have a spatial resolution of ~10km. Contrariwise, in our case the availability of a high-resolution wind field (300m) makes it possible to consider the spatial inhomogeneities due to variations in wind intensity and direction and, consequently, to improve the modeling of the marine circulation. Recent studies on the joint use of meteorological and sea (or lake) models have highlighted a significant enhancement in the representation of the main basin-scale motions if the shear stress description at the atmosphere-sea surface interface is improved (e.g., Amadori et al. 2018).

The meteorological field in the studied area is significantly influenced by the sea breeze regime (Gariazzo et al., 2007, Di Bernardino et al. 2016). As is known, when the synoptic wind is weak or absent, the wind field in coastal areas is governed for most of the year by the breeze regime, which typically shows spatial scales of tens of kilometers (Petenko et al., 2011, Pelliccioni et al. 2015). This fact, together with the presence of geographical features such as hills or mountains, can make the wind field quite inhomogeneous. The considerable differences in intensity and direction between the two wind roses depicted in Figure 3 clearly demonstrate this fact. The two wind roses were obtained based on the velocity data collected at the meteorological stations of Grottaglie and Marina di Ginosa during the year 2014. In Grottaglie (Fig. 3a), the wind is mainly from NNE and SWW, i.e. perpendicular to the coastline and coincident with the main direction of the sea and land breezes. Similarly, in Marina di Ginosa (Fig. 3b) the wind is aligned with NNW and SSE. This is further evidence that the hypothesis of wind with constant intensity and direction throughout the domain is far from being verified. This assumption could therefore cause significant errors in the simulations of the anemological field and, consequently, of the marine circulation, particularly when focusing on small regions, as in the present case.

CALMET uses a two-step approach to compute the wind field. The first step consists of the computation of the initial wind field on the basis of (i) measurements taken at the upper air stations, (ii) dimension of the chosen grid and (iii) topography and land use. In this way, kinematic effects of terrain, slopes and obstacles are considered. In the second step, CALMET adopts an inverse-distance method to perform the horizontal

spatial interpolation of the wind measured at the surface meteorological stations to each grid point of the computational grid and extrapolates the velocity to higher layers, using different parametric and similarity laws. The velocity divergence referred to all three-dimensional velocity components (carried out for each grid point) is minimized by calculating the mass unbalance and correcting the horizontal velocity components by means of an iterative process. The final velocity field is obtained when the divergence in each grid node is smaller than a user-specified threshold value. For more details, please refer to Scire et al. (2000).

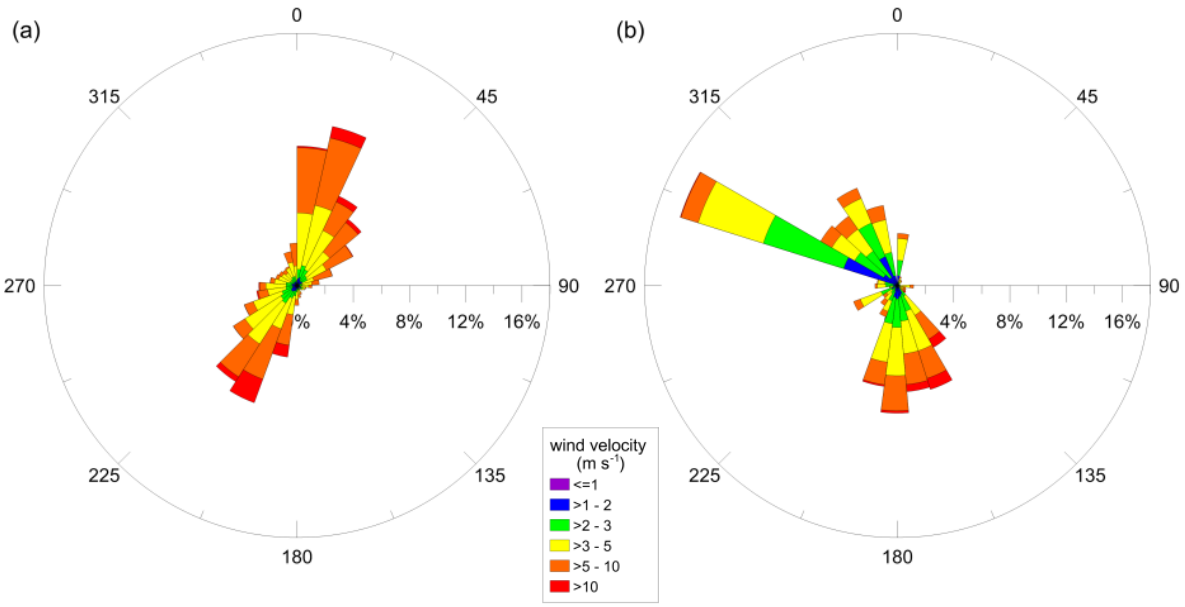

Figure 3: Annual wind roses for (a) Grottaglie, (b) Marina di Ginosa stations. Year 2014.

4.1.1 Boundary conditions for the meteorological runs

CALMET needs a series of input data, such as digital elevation model and land use category, in-situ measurements from surface meteorological stations and at least two vertical profiles of meteorological variables per day. In this study, we used data input related to the surface elevation from the Shuttle RADAR Topography Mission (SRTM), provided by NASA, with spatial resolution of 1 arc-sec (~30 m), while data provided by the Corine Land Cover CLC2000 (Level 2) with a spatial resolution of 100 m were employed for land use.

As is known, to evaluate reliable mass-consistent flow fields in complex terrain, it is fundamental to conduct the analysis using as many surface stations as possible. For this reason, the study domain investigated by CALMET included that of the hydrodynamic model and covered an area of approximately 3800 km^2, from 636 km to 709 km UTM East and from 4517 km to 4465 km UTM North (Fig. 4). The shape, size and position of the numerical domain used for the simulation was chosen based on terrain characteristics (i.e. shape and position of the coastline and terrain altitude) and wind regimes of the area of interest (prevailing and dominant winds come from NE and SE, respectively). The domain was discretized horizontally by a 243x173 regular grid along the x (longitude) and y (latitude) axis, with a spatial resolution of 300 m. Along the vertical, nine levels with spacing increasing with altitude were fixed to ensure an accurate analysis close to the ground,

where larger velocity and temperature gradient are expected to occur. In particular, the lowest model level height was at 10 m above the ground, i.e., the typical elevation of the surface meteorological stations. As previously mentioned, the simulations were carried out for the whole year 2014.

CALMET requires hourly data referred to the surface level, while it needs at least a vertical profile every 12 hours. Surface stations must be located within the domain, while the upper air data may also be external to it. In this study, ten surface meteorological stations, belonging to the networks managed by the Italian company for flight assistance, the regional agency for environmental protection (ARPA), the Italian tidal network, the Matera Space Geodesy center and by the Port Authority of Taranto, were taken into consideration. The surface stations were selected paying attention to their distance from the target basin and the availability of data for the whole simulated period. Most of them were located close to the basins of interest to ensure that the wind field simulations were as accurate as possible. The vertical profiles of the meteorological variables were taken from the upper air station launched every 12 hours from Brindisi Airport (ICAO code: LIBR) (not included in Fig. 4). Table 2 displays both the surface and upper air stations used for the numerical runs.

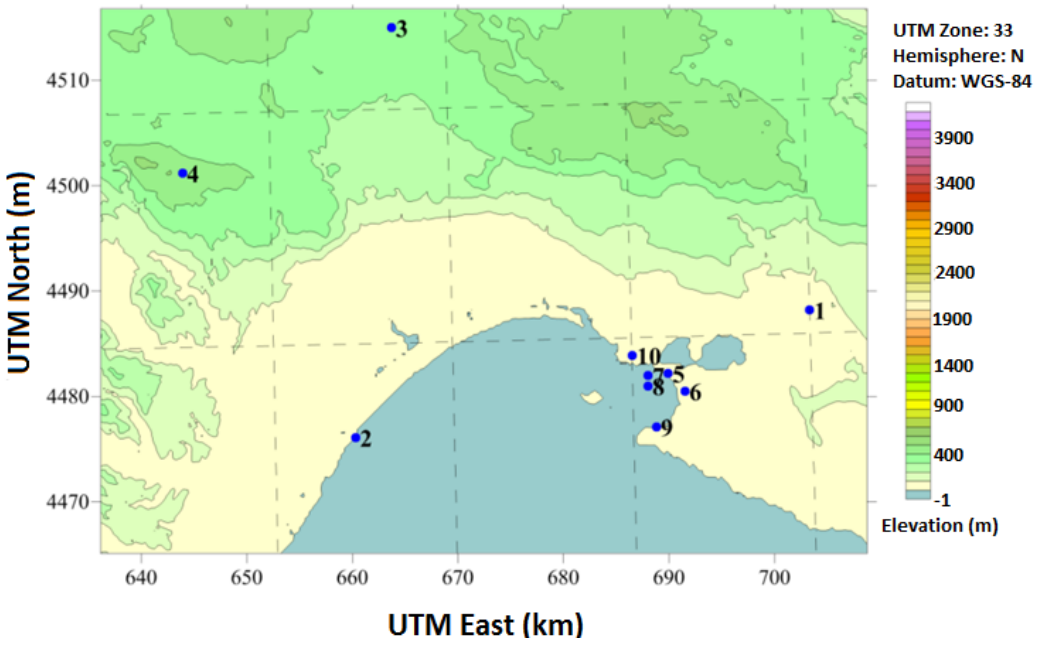

Figure 4: Domain investigated by CALMET and locations (blue dots) of the surface meteorological stations. The numbers indicate the station ID (see Table 2).

Table 2. Main characteristics of the selected meteorological stations.

Station ID	UTM East (km)	UTM North (km)	Elevation (m.a.s.l.)	Environment	Missing data
1	703.3	4488.2	69	airport	-
2	660.3	4476.1	12	airport	wind direction from 04/10/2014 to 09/25/2014
3	663.7	4515.0	350	airport	-
4	643.9	4501.2	483	rural	from 09/06/2014 to 11/05/2014

5	689.9	4482.2	42	urban	-
6	691.5	4480.5	40	urban	from 01/01/2014 to 07/12/2014
7	688.6	4482.0	10	marine	-
8	688.2	4481.0	6	marine	-
9	686.5	4483.9	n.a.	urban	-
10	688.8	4477.1	n.a.	urban	-
LIBR	801.0	4552.1	-	airport	-

4.2 Hydrodynamic model

SHYFEM is the hydrodynamic numerical model adopted in the present study. It is an open source code developed at the National Research Council - Institute of Marine Sciences of Venice (http://www.ve.ismar.cnr.it/shyfem). It consists of a finite element 3-D hydrodynamic model integrated by several modules for waves, sediment transport, Eulerian and Lagrangian tracer dispersion. The model solves the 3-D primitive hydrodynamic equations, vertically integrated on each layer, using a semi-implicit time stepping scheme that contributes to a stable solution of the equations. Details on SHYFEM can be found in Bellafiore and Umgiesser (2010). To compute water temperature and salinity field evolution, the model solves the transport and diffusion equations using a first order explicit scheme corrected by a total variation diminishing method. The model uses a k–ε turbulence closure scheme to compute vertical turbulent viscosities and diffusivities. For this aim, the module of GOTM (General Ocean Turbulence Model), described in Burchard and Petersen (1999), was adapted in the SHYFEM model. The finite element method for the horizontal discretization, with its unstructured grid approach, makes it possible to represent the complexity of coastal morphologies. In fact, it makes it possible to move from the lowest spatial resolution (open sea) to the higher one (ports, canals, bays, lagoons) gradually, without nesting different grids, and has already been successfully applied to different types of coastal ecosystems (Ferrarin et al. 2014).

4.2.1. Input and boundary conditions for hydrodynamic runs

The bathymetry of the basin (Fig. 5) up to a maximum depth of -200m was obtained by merging different data sets, subsequently interpolated on the numerical grid. In particular, we used: the bathymetry of the Mar Grande and Mar Piccolo digitalized by the Navy Hydrographic Institute (IIM) nautical charts; the Multibeam bathymetric data of the Mar Piccolo, supplied by ARPA-Puglia (Apulian Regional Agency for Environmental Protection); the bathymetry of the Gulf of Taranto provided by the Puglia Geographic Information System (www.sit.puglia.it).

The computation grid with triangular elements of the domain (Fig. 5b) was created by using the open source software GMSH (Geuzaine and Remacle, 2009) and consists of 15617 nodes and 29159 elements. The vertical discretization is in 21 z -levels and the spatial resolution ranges from 20 to 900 m. The numerical grid was improved with respect to previous studies (De Pascalis et al., 2016a,b) by adding the pylons of the Punta Penna bridge, shown in the enlargement of Figure 5b.

The annual simulation was performed with reference to the year 2014. The model was forced at the sea open boundary with temperature and salinity from E.U. Copernicus Marine Service Information and water level, measured at S. Eligio pier (Table 3) by the National Institute for Environmental Protection and Research (ISPRA). For freshwater inputs, the data adjusted after the calibration by De Pascalis et al. (2016b) were used, considering the yearly flow discharge of the sources quite constant (Table 3). The heat fluxes were computed by SHYFEM based on data (i.e. solar radiation, air temperature and humidity) measured by Station O (Fig. 1). Rain data were taken from the database of the Puglia Region Agency for Irrigation and Forestry Activities (http://www.agrometeopuglia.it/). The wind data, variable in space and time throughout the entire domain, resulting from the CALMET simulations were used to force the SHYFEM model.

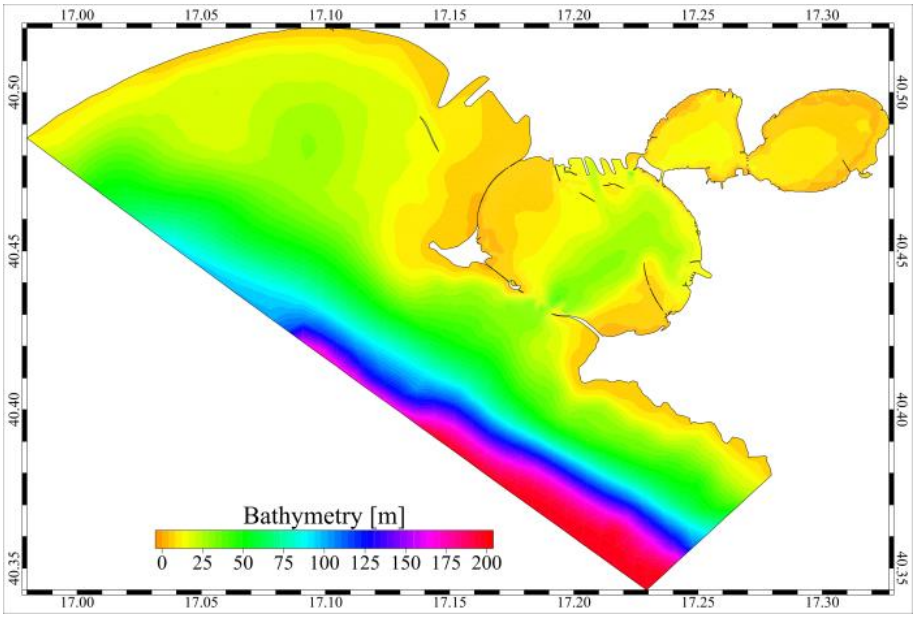

(a)

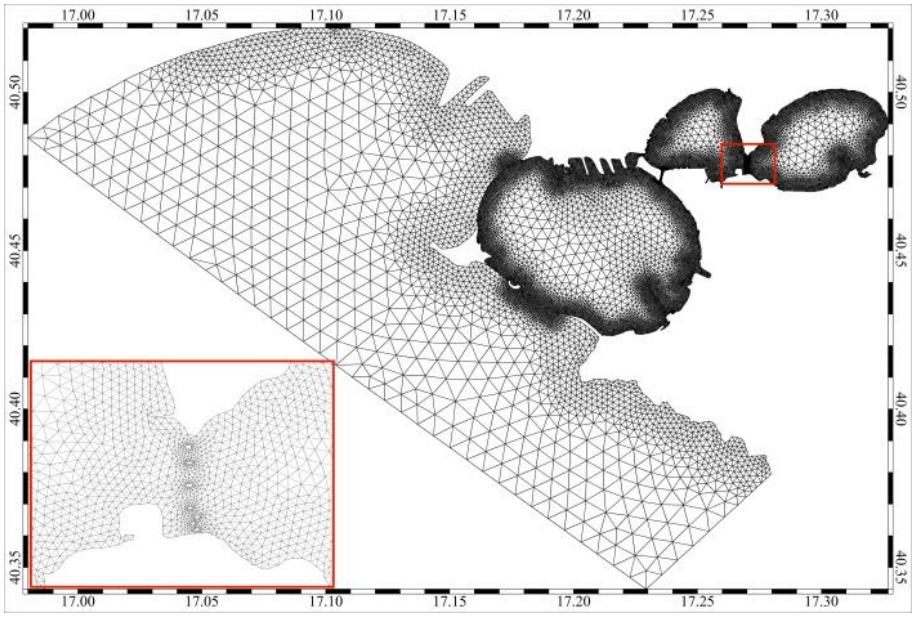

(b)

Figure 5: Bathymetry of the simulated domain (a); grid computing with zoom view on the pylons of the Punta Penna bridge (b).

The data concerning salinity (S) and temperature (T), supplied by COPERNICUS Service Products (http://marine.copernicus.eu/) and set as boundary condition at the open sea, were reprocessed using vertical interpolation programs, in order to be compatible with the 21 z-levels of the SHYFEM model. The initial conditions for T and S was set constant in all the basin (i.e. T=20 °C and S=37 psu). The time necessary to reach the dynamic equilibrium (spin-up time) for temperature and salinity is usually higher than that related to hydrodynamic velocities and water level, therefore, a spin-up time of one month (February 2014) was considered and the analysis of the 2014 results was then performed starting from March.

Table 3: Inflows /outflows used as input for the numerical simulation and picture of their locations in the target area from De Pascalis et al. (2016b)

Source	**Flux (m^3/s)**	**T (C∘)**	**S (PSU)**
Citro Galeso	1.2	19.7	3.8
Citro Le Copre	1.2	19.7	3.8
Citro Citrello	0.6	19.7	3.8
Citro S.Cataldo	2.0	19.7	3.8
Galeso River	0.8	18.1	2.7
D'Ajedda Canal	1.4	18	2.7
Battentieri Spring	0.4	18	2.9
Arsenale	0.5	20	2.7
Maricentro	0.014	20	2.7
Saram	0.004	20	2.7
65 Deposito	0.004	20	2.7
ILVA Waterpump	−27.22	ambient	ambient
ILVA 1	18.78	25	same as intake
ILVA 2	8.44	25	same as intake
ENI	2.7	25	2.7

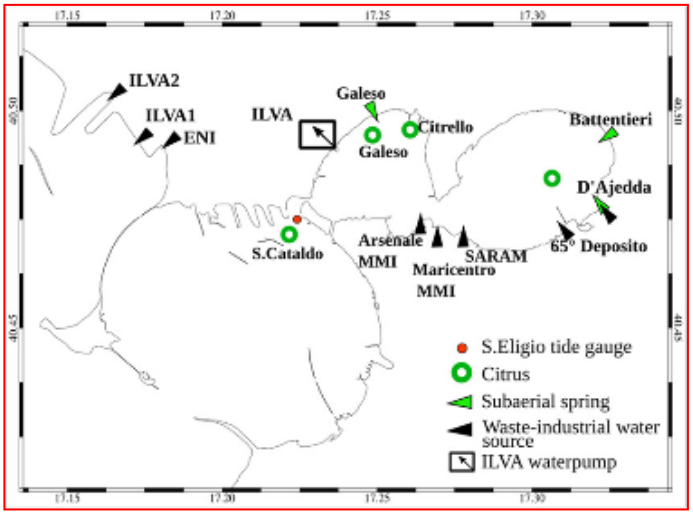

5. MODELLING VALIDATION AND RESULTS

As an example, Figure 6a illustrates the annual-averaged wind velocity field computed by CALMET for the whole domain at the lowest model level (10 m above the ground). The annual-averaged wind stress components τx (along W-E) and τy (along S-N) are also shown in Figures 6b and 6c, respectively. As previously mentioned, the shape of the coastline makes the target zone prone to high spatial variability of the wind. The noticeable inhomogeneity of the wind field calculated by CALMET, with dominant winds coming from NW and sinuously extending towards E, confirms that fact. In particular, a significant variability in wind direction and intensity is evident in both the Mar Grande and Mar Piccolo basins. This fact makes the need to use a meteorological model even more evident given the strong relationship between wind velocity and surface stress. Hence, simplified approaches based on the use of meteorological data collected from a single measuring station to force the hydrodynamic model could be inadequate in situations such as the one considered in the present work.

It is worth noting that CALMET and SHYFEM models were both calibrated in previous research (Di Bernardino et al., 2016; De Pascalis et al., 2016a, b). Thus, in this study the validation was operated at the end of the complete modelling procedure, that is by referring to the final results of the SHYFEM model (in turn forced with the results of the CALMET model). The data acquired in Station O (Fig. 1) and during the survey in BSs stations (Fig.2) were used for the comparison with the SHYFEM model outputs. Specifically, based on the dates of the survey, we decided to carry out the validation referring to the data acquired in November 2014.

(a)

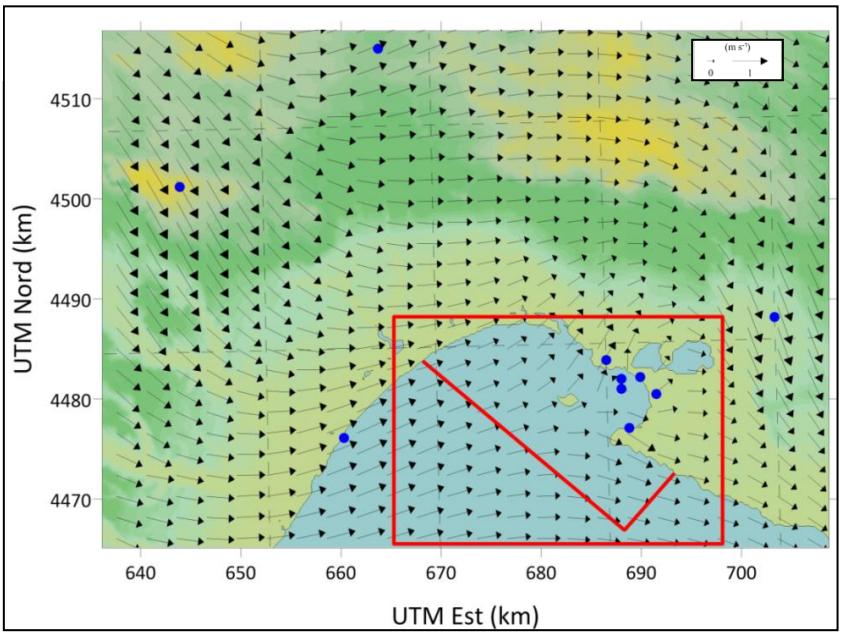

(b)

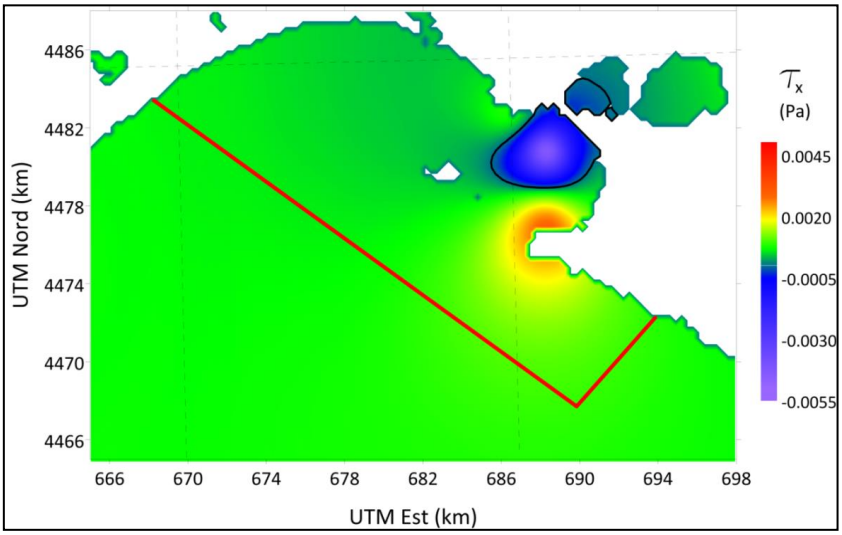

(c)

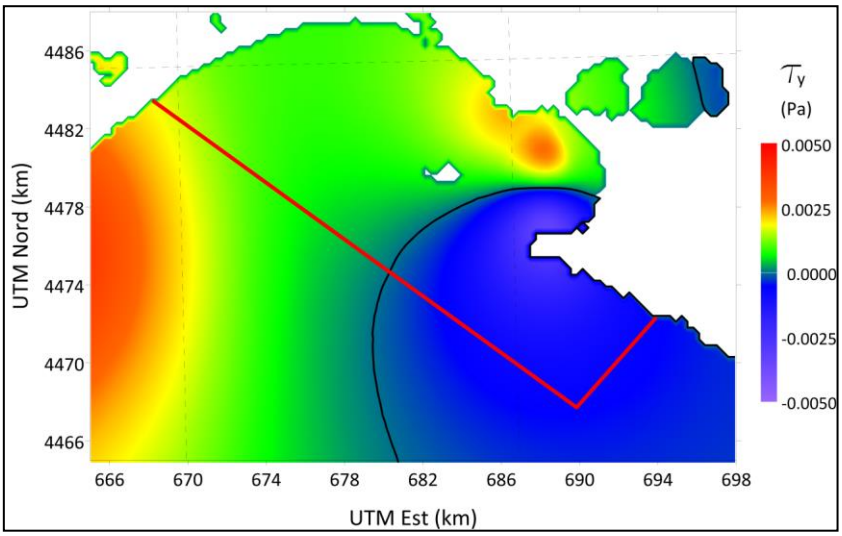

Figure 6: (a) Annual-averaged wind field over the whole CALMET domain, superimposed on topography. The red rectangle refers to the enlargements of panels (b) and (c), while the red line corresponds to the SHYFEM domain; (b) Annual-averaged field of the EW component of the surface shear stress; (c) As in (b), but for the NS component.

5.1 Validation procedure with data of Station N

The SHYFEM model current velocity outputs were compared with data measured in Station N of Navigable Channel (Fig. 1) during November 2014. Figure 7 shows the rose plots of the measured and modeled horizontal velocity for two representative depths, i.e. near surface (1.5 m from the sea surface) and near bottom (8.5 m from the sea surface). A double circulation in the Navigable Channel is evident, with prevailing outflowing currents near the surface and inflowing ones near the bottom. This aspect is well reproduced by the model.

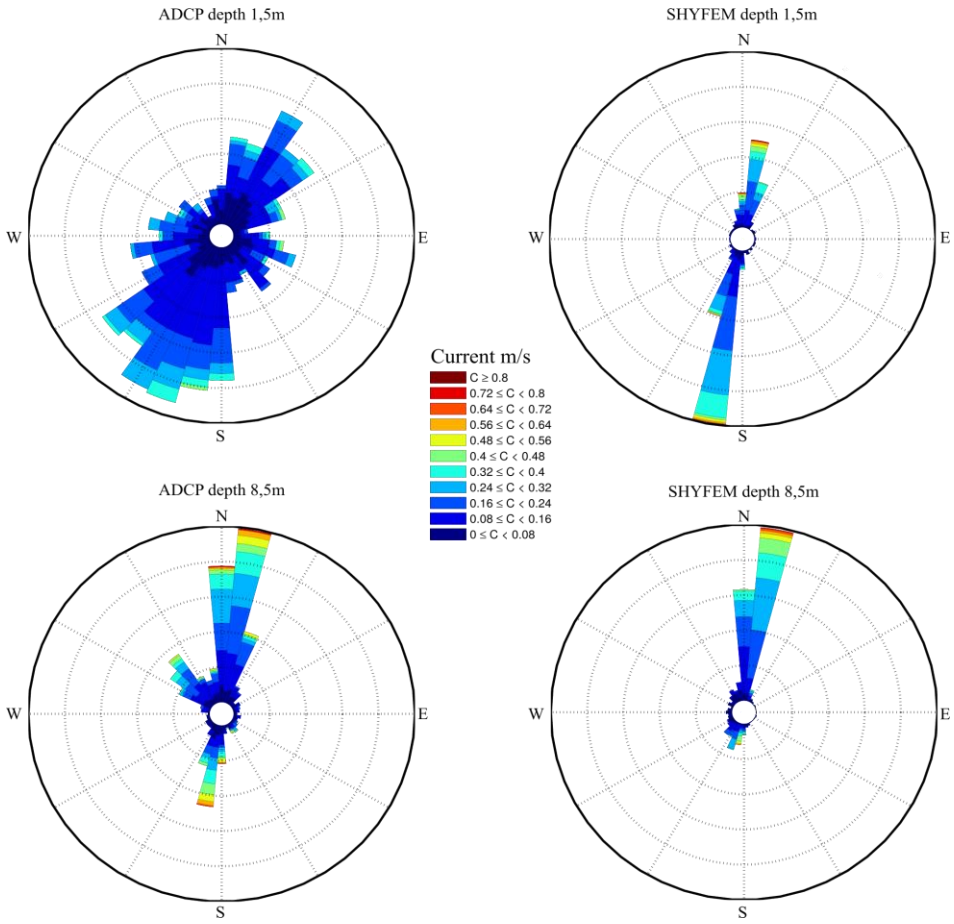

Figure 7: November 2014: rose plots of the measured (left column) and simulated (right column) currents for near surface and near bottom levels, in Station N. Direction of propagation shown.

The surface current roses measured by the ADCP shows a higher variability compared to their simulated counterparts. Nevertheless, the predominant direction (SW, i.e. exiting the Mar Piccolo towards the Mar Grande) and the velocities magnitude agree. With regard to the near bottom currents, the model is again able to reproduce the predominant direction (NE, i.e. towards the Mar Piccolo) and the current intensity. Specifically, the model does not precisely reproduce some peaks observed in the SSW direction at the bottom, as well as the surface variability around SW. In any case, considering the orientation of the Navigable Channel, the main flow along the NE-SW axis is correctly simulated. This can be detected from Figure 8 where the dispersion plots of the meridional velocity component (i.e. SN, positive northward), near the surface and near the bottom respectively, are displayed. The correlation between the two series of data is around 0.5 near the surface and around 0.8 near the bottom, thus meaning a better capability of the model to reproduce the near bottom dominant flow.

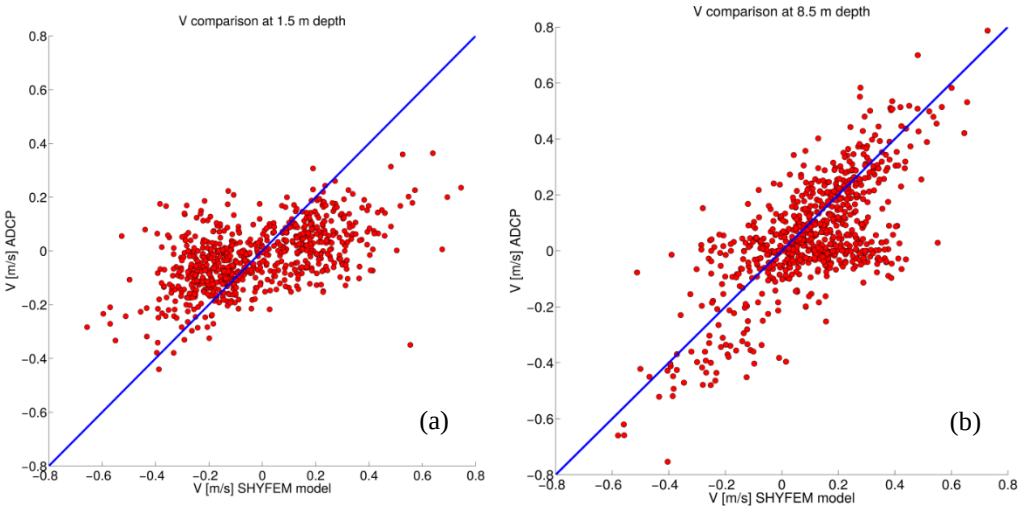

Figure 8: Dispersion plots of the meridional velocity component *V* for the month of November 2014 a) near surface and b) near bottom.

5.2. Validation with data of BS stations

In this case, to perform the comparison between the measured and the modelled profiles, the latter were extracted at the grid point closest to the actual measuring station points. Furthermore, both the zonal and the meridional velocity components were extracted for the corresponding acquisition time period of the field data. As an example, Figure 9a shows the comparison between the vertical profiles of the horizontal velocity vectors, both modelled and measured in station BS2 (Fig. 2), which are in the range 0.1÷0.4 m/s. Figure 9b displays the deviation between the modelled and measured velocity magnitudes at the corresponding depths.

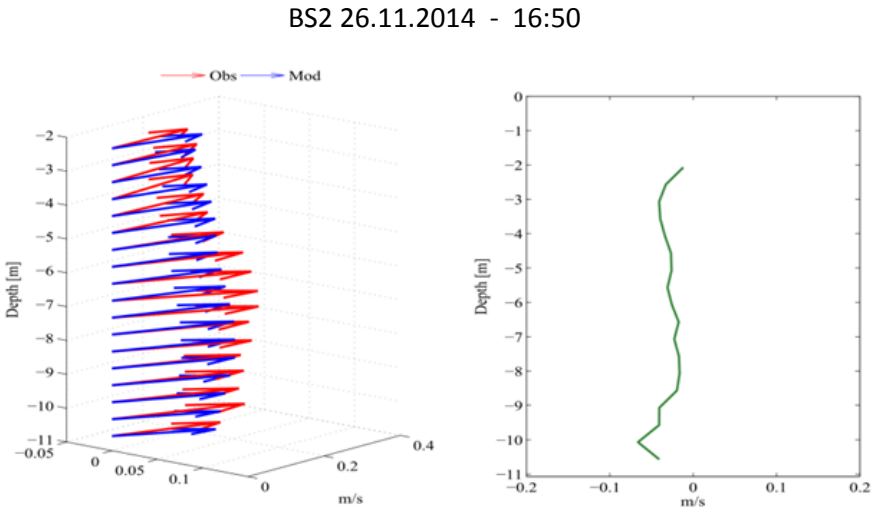

Figure 9. Comparisons between modelled and measured profiles of the horizontal velocity in BS2; a) horizontal velocity vectors and b) deviation between modelled and measured velocity magnitudes.

The numerical model is generally able to reproduce the main current and with greater accuracy in the middle part of the water column. In fact, it tends to slightly overestimate the velocity current in the upper layers, while it underestimates it near the bottom. The anticyclonic rotation of the vectors while deepening is also reproduced

by the model, but it is slightly over-shifted. For all the BS stations examined, the deviations in terms of magnitudes between the simulated and measured current velocity is ±0.10 m/s, indicating with negative values an underestimation of the model with respect to the measurement. This result is acceptable and satisfactory, considering that the discrepancies could be ascribed to several reasons, first the non-perfect adherence of the measuring station point to the grid node or the possible time shift between the measured value and the modeling output.

To validate the temperature (T) and salinity (S) variables, the SHYFEM results were compared with the observations sampled during the campaign on 26-27 November 2014 with the CTD. Figure 10 shows these comparisons as well as the differences between simulated and observed data (residuals), referring to stations BS1, BS3, BS4 only (Fig. 2) for the sake of brevity.

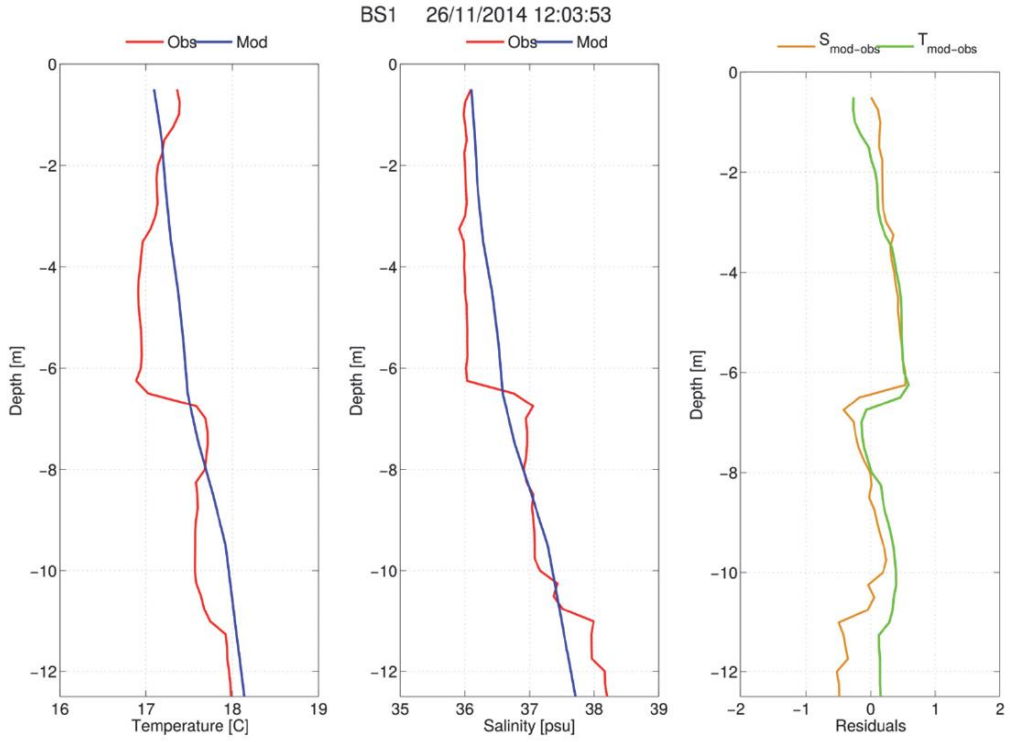

(a)

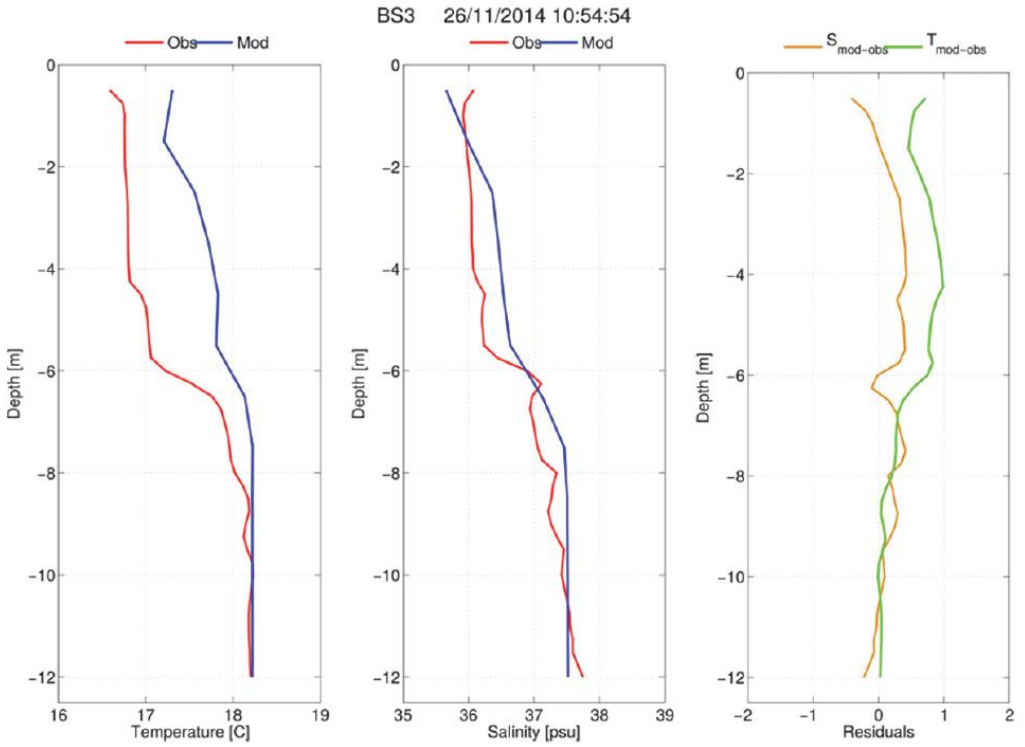

(b)

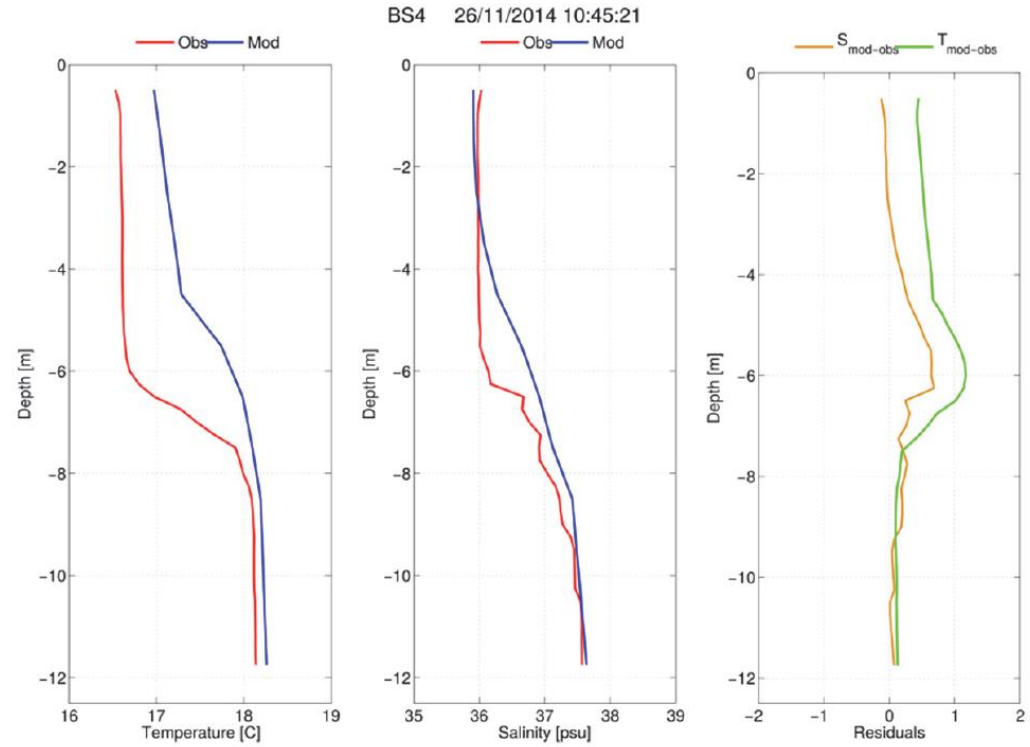

(c)

Figures 10. Comparison between the vertical profiles of T (left panel), S (center) and difference between simulated and observed data (right) at the station (a) BS1, (b) BS3, (c) BS4

Quite a good matching is noted referring to the vertical trends, which highlight for both T and S increasing values from the surface towards the bottom. For all the stations investigated low RMSE values are computed

(max RMSE for S is 0.45 and for T is 0.6 °C). Moreover, the residual values of T and S are always in the range [-1,1], thus demonstrating a good agreement between simulated and measured data.

5.3. Modelling results for current, temperature and salinity

As is known, temperature, salinity and density gradients, wind action, non-linear tidal interactions with basin morphology strongly influence the long-term circulation and pollutant transport. Therefore, the patterns of the surface and bottom annual-averaged currents are here examined. The residual circulation referred to the year 2014, depicted in Figure 10, shows a structure very similar to that reproduced by De Pascalis et al. (2016b) for the year 2013. In fact, the surface current tends to outflow from the Mar Piccolo towards the Mar Grande and the open sea (Fig. 11a), while there is an opposite behavior at the bottom (Fig. 11b). In general, the velocities on the entire water column are rather small, falling in the range of 0.02-0.10 m/s, with peaks at the bottom (0.2 m/s) near the Navigable Channel. The data of November 2014 (Fig. 8) also confirm this double bottom-surface circulation.

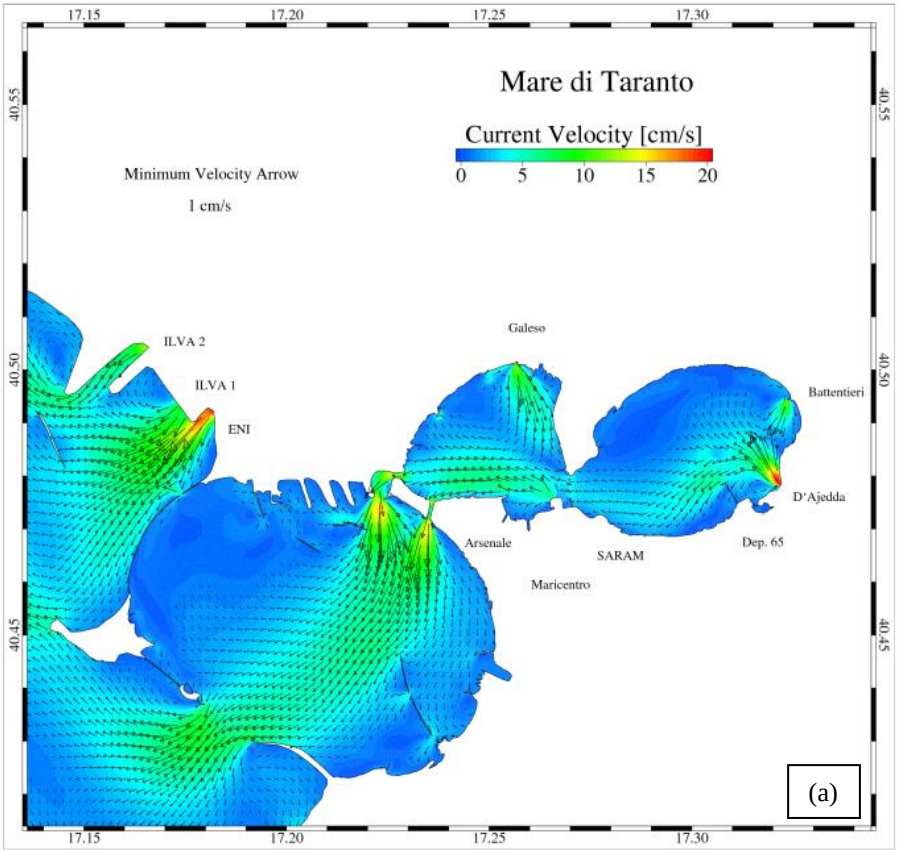

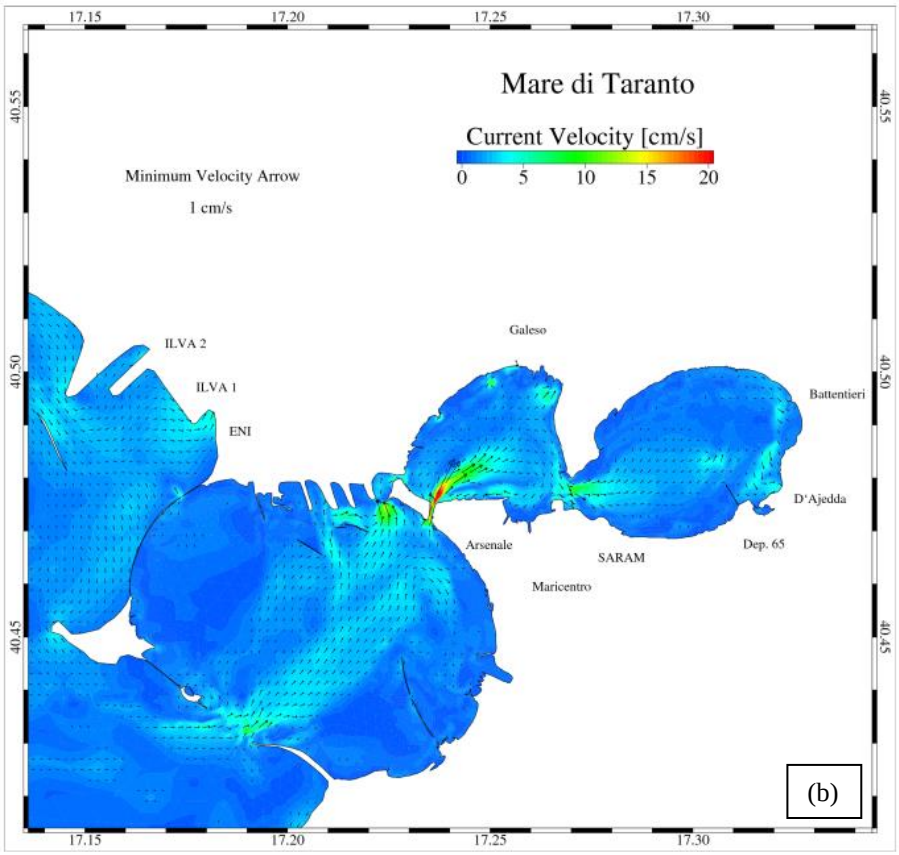

Figure 11: Zoom view of the annual-averaged horizontal currents simulated by SHYFEM (a) near surface; (b) near bottom.

To detect the annual-averaged vertical stratification of salinity and temperature, a surface-to-bottom difference was computed for T and S in each node of the domain (Fig. 12): negative values of the difference mean higher values of these scalar variables at the bottom, while positive values mean higher values at the surface. In general, a pronounced stratification for both salinity and temperature is observed near the industrial discharges outside the Mar Grande (ENI, ILVA1, ILVA2) as well as near Galeso and Citrello submarine springs in Bay I of the Mar Piccolo (Tab. 3). In the Mar Piccolo, the salinity at the surface is lower than at the bottom by about 2.2 psu in Bay I and 1.5 psu in Bay II. In the Mar Grande the salinity gradient is lower than 0.8psu (Fig. 12a). The presence of citri and urban discharges, especially in the Mar Piccolo, induces a salinity gradient decreasing from its bays towards the Mar Grande and the open sea.

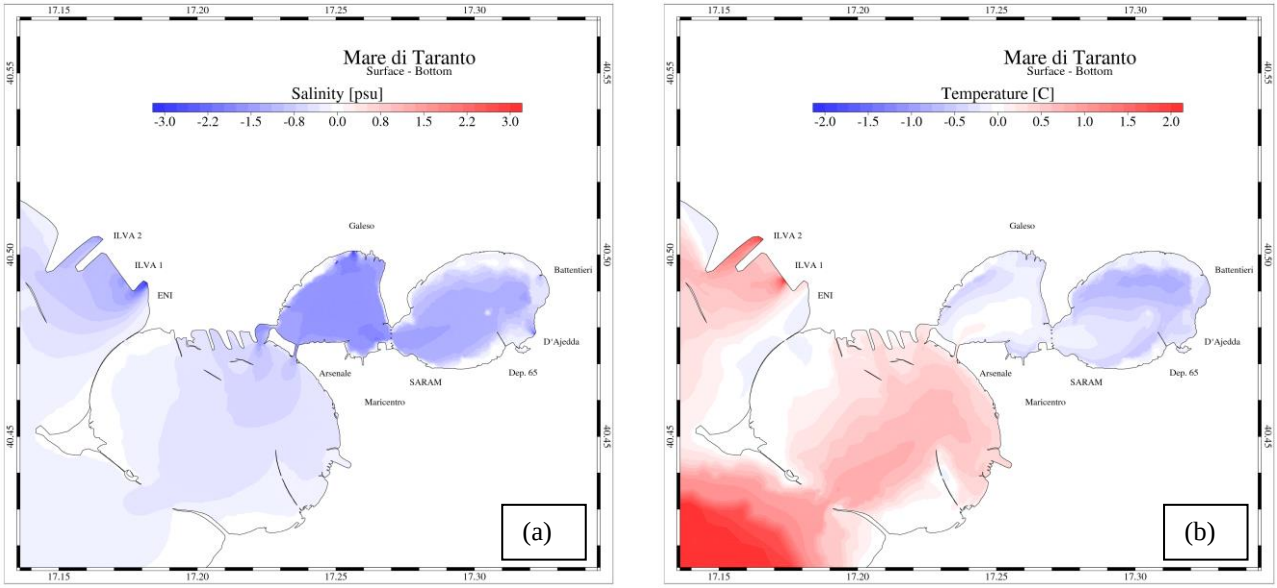

Figure 12. Gradient of salinity (a) and temperature (b) from surface to bottom. Annual averaged values of 2014.

Vertical temperature gradient values fall in the range of 0.2-1 °C range (Fig. 12b). Specifically, in the Mar Grande the annual-averaged temperature at the surface exceeds the near bottom one by about 0.5-1 C°, while in the Mar Piccolo the opposite occurs. In fact, due to its lower depth, the Mar Piccolo responds much more rapidly to the atmospheric forcing, consequently regulating its temperature, while the Mar Grande is more influenced by the vertical stratification. This leads to a stable stratification with saltier and colder water near the bottom, coming from the open sea, and less saline and warmer water (i.e. less dense water) near the surface. This peculiar horizontal and vertical density distribution gives rise to a long-term estuarine circulation, confirming what found by De Pascalis et al. (2016b) with reference to 2013.

6. TIME SCALE INDICATORS

The knowledge of the main features of the water fluxes in the basin allows us to obtain a clear picture of the transport and spreading processes of polluting substances and sediments. A vigorous water exchange between a semi-enclosed basin and the open sea could guarantee a rapid replacement of its water mass and some protection from pollution events. Depending on the ability to renew water masses, the basin is more or less vulnerable to pollution hazards. Moreover, it could also define the role of the basin in terms of nutrient distribution and trophic net, ecosystem productivity, nursery and connectivity propensity (Gulorget and Perthuisot 1992; Ghezzo et al. 2015). As described in the following, relating the basin hydrodynamics to such phenomena is possible if we focus on some specific indicators, specifically linked to two different time scales. These indexes are not easily measurable in the field and numerical modeling tools must be used to quantify them. In the present study, a Lagrangian module was added to the main SHYFEM code to carry out particle tracking applications (De Pascalis et al, 2016a). The Lagrangian module was tightly integrated into the hydrodynamic framework and run on the same unstructured grid as SHYFEM itself, to avoid the numerical diffusion due to the interpolation of velocities onto different grids. This module provides the particle trajectory,

i.e. the position of the particle at the new time step, as a function of the position at the previous time step and the displacement due to both the advective velocities (given by the current field) and the ones given by the turbulent diffusion. This computation was done in all three directions, so the module differs from previous research where it was limited to the 2D case (Cucco and Umgiesser, 2006, Bellafiore et al., 2008; Cucco et al., 2009). Thus, referring to the time scale indicators, the added value of the present study lies in the fact that they were calculated all (i.e. WRT, WTT and TI), and specifically the TI was calculated in its 3D version. Further, they are all based on an annual time scale (i.e. 2014).

6.1 Water renewal time and water transit time

Over the years, many studies have dealt with the concept of water renewal time (WRT) and water transit time (WTT) (Zimmerman, 1976; Takeoka, 1984; Sanford et al., 1992; Luketina, 1998; Wang et al., 2004). The WRT is a time scale based on a Eulerian reference system and is defined as the time needed to replace with clean water the mass of a conservative tracer, originally released in the domain in each element and layer of the computational grid (Cucco et al., 2009, Cucco and Umgiesser 2015). In our study, the water coming from the open sea and from the submarine and surface springs was fixed with tracer concentration equal to zero. This useful factor characterizes the system in terms of renewal capacity and resilience, especially with reference to potential pollution phenomena (Kjerfve, 1989, Umgiesser et al. 2004, Ferrarin et a. 2014). Furthermore, being related to the exchange of water masses, it could be a vector for different types of materials (oil, debris, etc.) (Jordi et al., 2006, Davidson et al., 2009). The knowledge of this transport time scale can also help to understand the complex behavior associated with bio-geo-chemical phenomena (Ghezzo et al., 2011).

The WTT is a time scale based on a Lagrangian reference system. It is defined as the time required by a particle, seeded in each grid element and vertical layer, to exit from the domain reaching the open sea (Bolin and Rodhe, 1973; Zimmerman, 1976; Dronkers and Zimmerman, 1982; de Kreeke, 1983; Prandle, 1984, Cucco and Umgiesser 2015). This value is typical of the point where the particle is initially released. Hence, conceptually, the two transport time scales are different. In fact, the WRT is a feature of the area under examination and of the main hydrodynamic patterns, indicating how long it takes to exchange water masses with new water coming from both the sea and the rivers discharging into the basin. Instead, the WTT is a characteristic of the single particle flowing into the basin until it leaves it and therefore it essentially depends on the number and initial positions of seeded particles. In this study about 10^7 of passive particles were released on 1 March 2014 homogeneously (vertically and horizontally) inside the Mar Grande and Mar Piccolo basins in order to have statistical robustness for the computed trajectories. Details on the Lagrangian method used are in De Pascalis et al. (2016a).

6.2. Trapping index

Although significant, the WRT and WTT time scales represent two different aspects of the transport dynamics of the system, thus high values of WRT and WTT do not always identify the areas where the water masses remain trapped and the exchange is poor. To better characterize areas of stagnation, Cucco and Umgiesser

(2015) proposed a new dimensionless index in a first 2D version, called Trapping Index (TI), which is defined as the normalized product between the water renewal and transit times. This allows the identification of areas where both these time scales are high, as well as hot spots where water masses might be especially vulnerable to pollution. A first attempt to define a 3D TI was made by De Pascalis et al. (2016a), nevertheless it provided vague results, being the computation applied to a very short temporal period of investigation, that is two months. In this work, TI is extended to the 3D case on an annual scale and calculated at each point of the domain for each vertical level according to the formula:

$$TI = \frac{WRT \cdot WTT}{WRT_{\max} \cdot WTT_{\max}} \qquad (1)$$

where the subscript *max* indicates the overall maximum values of WRT and WTT in the basin. As a result, TI ranges from 0 to 1, meaning increasing water stagnation.

The trapping index is expected to be large only in areas where both residence time and transit time are large. In areas where one of these time scales is large and the other is small, the trapping index will also be small. It will be negligible in areas where both time scales are small. It is therefore possible to easily identify areas that show high residence and transit times, e.g., areas that have a small tendency to exchange water with the surrounding areas and that can be identified with water masses trapped in the basin.

Figure 13 displays the WRT mapping at surface and near bottom levels, for the year 2014. Analogously to the salinity and temperature distributions, also in this case we can observe the different behaviour of the three sub-basins (i.e. Bay II, Bay I and the Mar Grande). The longest renewal time characterizes Bay II, with values around 40 days. The WRT decreases to around 32 days in Bay I and finally to 12 days in the Mar Grande. The vertical distribution corroborates the estimates computed for the year 2013 by De Pascalis et al. (2016b), showing surface waters that have the tendency to stagnate more with respect to the bottom ones. In fact, due to the intense inflow from the open sea, bottom waters are replaced even 10 days faster than the surface waters.

Figure 14 shows the distribution of the WTT near the surface and the bottom layer. As a general consideration, the WTT map shows a higher spatial variability with respect to that experienced by WRT, which is due to the chaotic Lagrangian effect and to the initial seeding of particles, not comparable to the Eulerian continuum of tracer concentration (Cucco et al. 2006). The WTT distribution highlights that the Lagrangian particles released in the surface layer of the Mar Grande are transported offshore faster than the ones released at the bottom (Fig. 14), because of the intense outflowing at the surface (Fig. 11). This is especially true in the Mar Grande where this time difference reaches even twenty days. In Bays II and I we note a similar behavior, but the difference between surface and bottom WTT values is halved, based on current intensities more comparable along the depth.

Figures 15a and 15b show the TI index plotted on the surface and bottom layers respectively. In both cases, its distribution confirms the intuitive characterization for the three sub-basins from the most retentive (Bay II) to the one with highest rate of water exchange with the open sea (Mar Grande). Moreover, some hot spots are evident in the three sub-basins. At the surface are to be found (Fig. 15a): i) in the Mar Grande, the Port area, due to the presence of docks and piers which are obstacles to water flowing, and the south-eastern inlet where

the southern shore at the Navy base is located; ii) in Bay I, the large retentive zone that extends from the Navy Arsenal (Fig. 2) to the ILVA water pump, serving the industrial refrigeration system; iii) in Bay II, characterized by an even more retentive central area, the small inlet neighbouring the D'Ajedda channel (Table 3). Near the bottom (Fig. 15b) we generally observe lower values of TI with respect to the surface, consistently with both the WTT and the WRT distributions. The highest TI values of the basin are concentrated in Bay II, in particular along the shoreline, as expected, considering that these are the shallowest areas of the domain. Analogously to the surface, also at the bottom the hot spots with the largest values of TI are the inlet close to the D'Ajedda channel and the one of the Navy base.

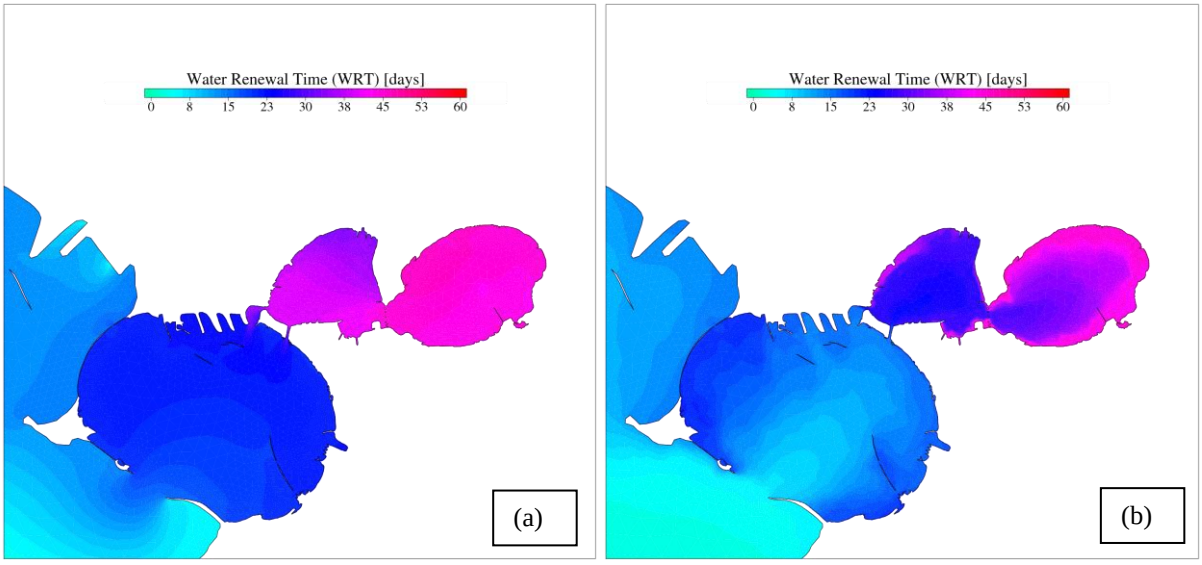

Figure 13: Distribution of WRT a) near surface and b) near bottom

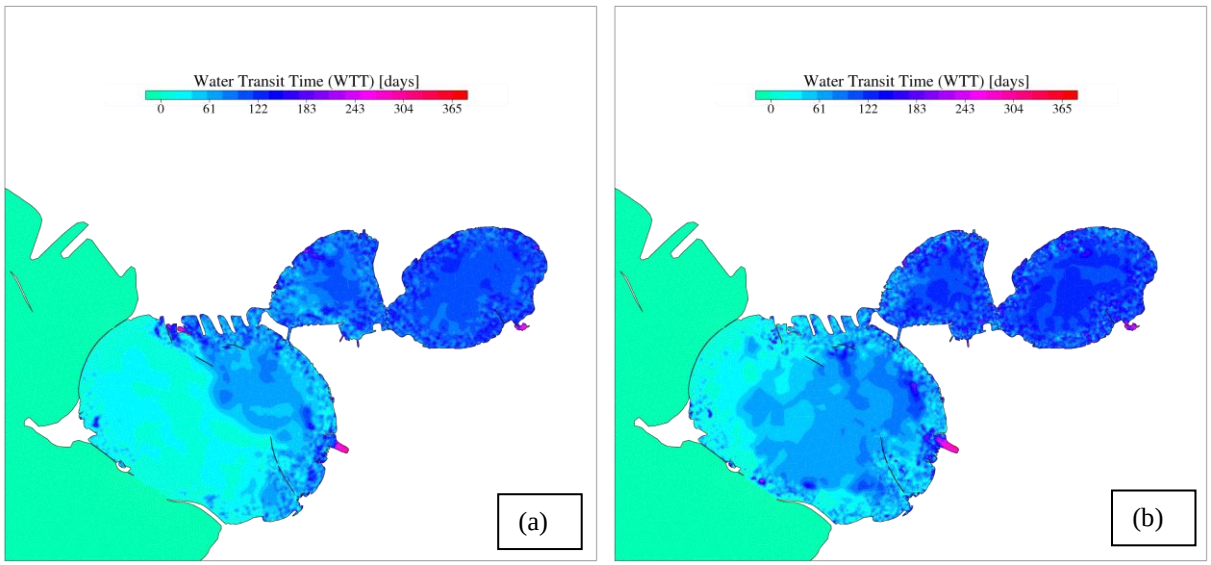

Figure 14: Distribution of WTT a) near surface and b) near bottom

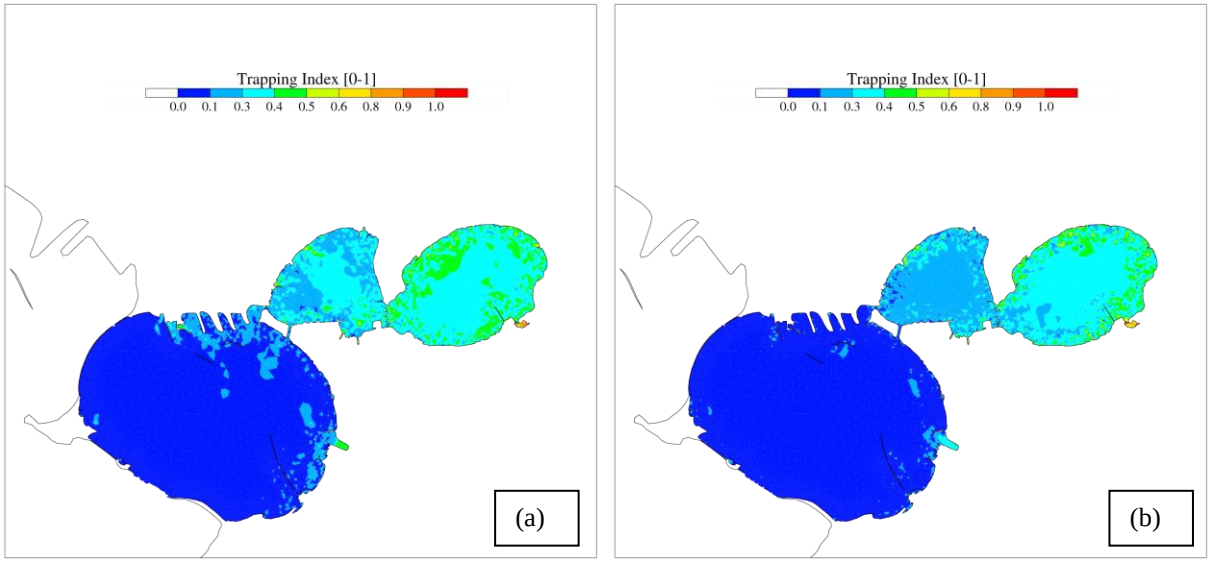

Figure 15: Distribution of TI index a) near surface and b) near bottom

7. DISCUSSION

The hydrodynamic and thermohaline results described in the previous sections confirm an established baroclinic estuarine circulation through the three sub-basins, as already found by De Pascalis et al. (2016b). In any case, it is worth noting that De Pascalis et al. (2016b) reached this conclusion by forcing their numerical model with the data of 2013, while in our modelling we used the data of 2014. Accomplishing an analogous result is thus meaningful, because it highlights that, on the annual temporal average, the hydrodynamic and thermohaline patterns in the basin have a recurrent, established and typical behavior. In fact, the annual-averaged trends of surface (Fig. 11a) and bottom currents (Fig. 11b) highlight the presence of a dual opposite circulation with different patterns. In fact, two different water masses can be recognized: the salty and cold water entering the system on the bottom layer and the less salty and warmer water outward directed on to the surface (Fig. 12). In this case, the role of the estuarine circulation engine, generally played by the river in a typical estuary, is attributable to submarine and subaerial freshwater springs, while the bottom current represents the salt-wedge entering the system from the open sea. In particular, in the present study, these hydrodynamic patterns are validated based on the velocities measured by both the fixed Station N and during the survey, obtaining a satisfactory matching. Previous researches used salinity and temperature data to validate indirectly their numerical velocity fields (De Pascalis et al., 2016b). It is also important to point out that the hydrodynamic model has been forced at the sea surface by using the wind-stress components coming from the meteorological model CALMET. Such a choice of boundary conditions is motived by the fact that wind speed and direction measured by a single meteorological station cannot be considered representative of the wind field present on the whole area of interest, despite the limited size of the basin (see Fig. 3). It is worthwhile mentioning that one of the strong points of diagnostic models like CALMET is that of being able to perform simulations with relatively small computational costs even in the case of high spatial resolution. In the present work, the latter is 300 m, which is much higher than that generally adopted in numerical weather prediction (NWP) models, which represent an alternative to diagnostic models (see e.g. Zannetti 1990). NWPs are generally used to

forecast the time evolution of the atmosphere through the numerical integration of the equations of fluid mechanics that describe the dynamics and thermodynamics of gases. However, NWP models require much larger computational costs and their use in complex situations is not straightforward (see e.g. Valerio et al. 2017).

These findings allowed us to evaluate some proper time scales strongly related to the hydrodynamics of the system, i.e. the WRT and the WTT times. Especially the WTT time is a novel parameter computed for an annual temporal period for the whole domain. In fact, Umgiesser et al. (2004) examined only the Taranto Seas WRT time for the year 2005 limited to a 2D approach. De Pascalis et al. (2016b) described only the annual-averaged WRT distribution for the year 2013 in both the Mar Piccolo and the Mar Grande basins but did not analyze the WTT time nor the TI index. The trend of the WRT time obtained in the previous research is confirmed by our study: the effect of the bottom marine water intrusion is to accelerate the bottom layer water exchange on average by ten days.

Nevertheless, by now analyzing also the WTT time, we observed that the surface Lagrangian transport directed outside the domain is much faster than the bottom one, with a remarkable time difference (10-20 days). Therefore, it is worth noting that a single time scale, i.e. only the renewal time or only the transit time, could offer a misleading perception of the real situation. In fact, finding high values of one of these time scales might not necessarily mean a slow water exchange. Indeed, a high renewal time but a low transit time might be caused by water masses that pass through the area but come from other zones (Cucco and Umgiesser, 2015). For this reason, the TI trapping index, which is the simple normalized product between the residence and the transit time, was introduced. It is also worth observing that this index is only based on the hydrodynamics of the basin and not on chemical or biological parameters directly related to the water quality. Based on the values assumed by the TI index and comparing them along the vertical, we mapped the areas of potential trapped water masses and consequently the hot spots, as being very exposed to pollution and scarce water quality, on annual-average. They are displayed in Figure 16, with increasing numbering as their sensitivity increases and result from the comparison between the superficial and near bottom distributions of TI, based on the highest values observed. The procedure of the macro-zonation consists in the following phases. We divided the total basin in subareas of order of magnitude $O(10^4)$ m^2. For each subarea, the spatial average of the TI values was calculated. This operation applied to both surface and bottom TI distributions. After this, for each subarea, we compared the averaged superficial and bottom TIs and assumed the maximum of the two as the TI data to be plotted in the sensitivity map.

The largest part of the Mar Grande (area 1 in Figure 15), positively affected by the exchange flows with the open sea, is the least exposed to possible retention (with TI in the range of 0-0.1). Two more sensitive areas in the Mar Grande, with TI in the 0.1-0.3 range, are the Port area, where docks and piers intercept and slow the flow, and the south-eastern inlet hosting the Navy base, due to its topographic configuration. The same level of sensitivity is identified in Bay I along the northern coast and in the southern part, near the connection with the two channels. They are all marked as areas 2. The central part of Bay I, as well as that of Bay II, are characterized by higher sensitivity to stagnation, with TI in the 0.3-0.4 range (areas 3). A higher sensitivity is

noted in areas 4 (TI in the 0.4-0.5 range), along the whole shoreline of Bay II and in two hot spots of Bay I, i.e. near the ILVA pumping system and the Naval shipyard. The inlet neighbouring the D'Ajedda channel is the most sensitive area (area 5), due to its TI values greater than 0.5, because of its topographic shape and depth. Based on Figure 16, a sort of hierarchy in the zones most exposed to a potential degradation is thus established.

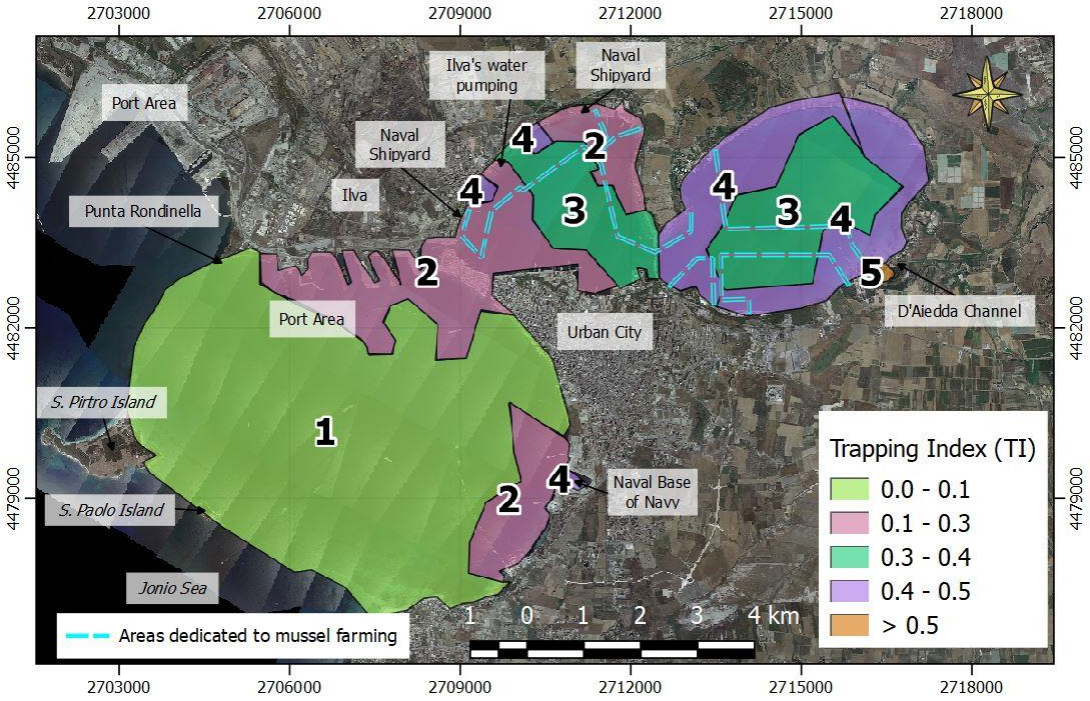

Figure 16. Sensitive areas mapped in Mar Grande and Mar Piccolo basins

8. CONCLUSION

In heavily anthropized and confined coastal basins the identification of areas most exposed to human activities and pollution events is a priority aspect in decision planning and coastal management. For this purpose, in the present study, the meteorological CALMET model and the hydrodynamic SHYFEM model were used in conjunction, to i) deduce the main physical processes typical of the Mar Grande and Mar Piccolo system; ii) identify the time scales related to these processes, such as the WRT and the WTT times; iii) detect the areas most exposed to potential pollution, based on the TI index.

The validation of the modelling procedure was carried out referring to the results of the SHYFEM model, in turn forced with the results of the CALMET one. For this scope, the available field data of current, temperature and salinity measured in Station N (Fig. 1) and in stations BSs (Fig.2), for the month of November 2014, were used. The main results of the validation highlight that, referring to velocity, the correlation values are around 0.5-0.8, indicating that the numerical model is generally able to reproduce the main current along depth. As for T and S, their residuals are in the range [-1,1], thus demonstrating a good agreement between simulated and measured data. The results of the validated model demonstrated that the system has a typical horizontal

and vertical density distribution giving rise to a long-term estuarine circulation, confirming previous research (De Pascalis et al. 2016a,b).

The key parameters assessed in order to identify possible sensitive areas subject to stagnation were the water renewal time and the water transit time, which are strictly related to the hydrodynamic patterns in the basin. They showed that for a complete water renewal in Bay II forty days are needed, only twelve are needed for the Mar Grande. Moreover, the flowing of Lagrangian particles released in the surface layer is generally faster than near the bottom. To have more complete information, a trapping index TI, based on both WRT and WTT, was identified. This index allowed us to map areas with different levels of sensitivity in the system and thus to recognize a sort of hierarchy. Specifically, in the Mar Grande two hot spots are observed: the Port area and the south-eastern inlet hosting the Naval base. In Bay I, we detect two other hot spots near the ILVA pumping system and the Naval shipyard. Bay II is characterized by high sensitivity along the whole shoreline, with the inlet neighbouring the D'Ajedda channel found to be the area most exposed to a potential degradation. Based on these results, it is evident that particular care should be paid to the planning of periodic monitoring actions to safeguard the system.

Acknowledgments: The monitoring stations were set up in the framework of the RITMARE project with funds from PON R&C 2007-2013. The present work was funded by an agreement between the Polytechnic University of Bari and the Special Commissioner for urgent measures of reclamation, environmental improvements and redevelopment of Taranto, gratefully acknowledged.

Author Contribution: VC, GC, RV and MM funded the research; MM supervised the research and conceived the experimental apparatus; GL, PM and MM conceived and coordinated the activities; EA, FDP, FDS, ADB and AP performed the numerical modelling and analyzed the results; EA and FDS wrote the paper; EA, MBM, DDP, FDP, FDS, ADB, GL, PM, MM and AP discussed and revised the paper.

REFERENCES

Amadori, M., Piccolroaz, S., Giovannini, L., Zardi, D., Toffolon, M., 2018. Wind variability and earth's rotation as drivers of transport in a deep, elongated subalpine lake: The case of Lake Garda. Journal of Limnology 77, 505-521.

Armenio, E., Serio, F. De, Mossa, M., 2016a. An approach for data-driven characterization of tide and current fluxes in coastal basins. Hydrology and Earth System Science, 21, 1–14.

Armenio, E., Ben Meftah, M., Bruno, M.F., De Padova, D., De Pascalis, F., De Serio, F., Di Bernardino, A., Mossa, M., Leuzzi, G., Monti, P., 2016b. Semi enclosed basin monitoring and analysis of meteo, wave, tide and current data Proc. IEEE EESMS 2016: 180-185; ISBN: 978-1-5090-2369-1

Armenio, E., De Padova, D., De Serio, F., Mossa, M., 2017. Monitoring system for the sea: Analysis of meteo, wave and current data. IMEKO TC19 Workshop on Metrology for the Sea, MetroSea 2017: Learning to Measure Sea Health Parameters 2017-October, 143-148

Armenio, E., De Padova, D., De Serio, F., Mossa, M., 2018. Monitoring System in Mar Grande Basin (Ionian Sea). Proc. IEEE International Workshop on Metrology for the Sea, Proc. 8657891: 104-109, doi: 10.1109/MetroSea.2018.8657891

Armenio, E., Ben Meftah, M., De Padova, D., De Serio, F., Mossa, M., 2019. Monitoring Systems and Numerical Models to Study Coastal Sites. Sensors, vol. 19(7), 1552

Bellafiore, D, Umgiesser, G., 2010. Hydrodynamic coastal processes in the North Adriatic investigated with a 3D finite element model. Ocean Dynamics 60 (2), 255-273

Bellafiore, D., Umgiesser, G., Cucco, A., 2008. Modelling the water exchanges between the Venice Lagoon and the Adriatic Sea. Ocean Dyn 58, 397 – 413.

Bolin, B., Rodhe, H., 1973. A note on the concepts of age distribution and transit time in natural reservoirs. Tellus 25, 58–63. DOI: 10.1111/j.2153-3490.1973.tb01594.x

Burchard, H., Baumert, H. (1995) On the performace of a mixed-layer model based on the turbulence closure. J. Geophys. Res. (C5), 100, 8523-8540.

Cannata, G., Barsi, L., Petrelli, C., Gallerano, F., 2018. Numerical investigation of wave fields and currents in a coastal engineering case study. WSEAS Transactions on Fluid Mechanics, 13, 87-94.

Cardellicchio, N., Annicchiarico, C., Di Leo A., Giandomenicom S., Spada, L., 2016. The Mar Piccolo of Taranto: an interesting marine ecosystem for the environmental problems studies. Environ Sci Pollut Res. 23(13), 12495-501.

Cucco, A., Umgiesser, G., 2006. Modeling the Venice Lagoon residence time. Ecol Model 193(1–2):34–51.

Cucco, A., Umgiesser, G., 2015. The Trapping Index: How to integrate the Eulerian and the Lagrangian approach for the computation of the transport time scales of semi-enclosed basins. Mar Pollut Bull, 98(1-2), 210-20.

Cucco, A., Umgiesser, G., Ferrarin, C., Perilli, A., Melaku Canu, D., Solidoro C., 2009. Eulerian and Lagrangian transport time scales of a tidal active coastal basin. Ecological Modelling, 220(7), 913-922.

Cucco, A., Perilli, A., De Falco, G., Ghezzo, M. Umgiesser, G., 2006. Water Circulation and Transport Time Scales in the Gulf of Oristano. Chemistry and Ecology, 22 (Suppl. 1), S307-S331.

Davidson, F. J. M., Allen, A., Brassington, G. B., Breivik, O., Daniel, P., Kamachi, M., Sato, S., King, B., Lefevre, F., Sutton M., Kaneko K., 2009. Applications of GODAE ocean current forecasts to search and rescue and ship routing. Oceanogr, 22, 176– 181.

De Carolis, G., Adamo, M., Pasquariello, G., De Padova, D., Mossa, M., 2013. Quantitative characterization of marine oil slick by satellite near-infrared imagery and oil drift modelling: the Fun Shai Hai case study. International Journal of Remote Sensing, 34, 1838 -1854.

De Kreeke, J. V., 1983. Residence time: application to small boat basins. Journal of Waterway, Port, Coastal and Ocean Engineering 109 (4), 416–428.

De Padova, D., Mossa, M., Adamo, M., De Carolis, G. Pasquariello, G., 2017. Synergistic use of an oil drift model and remote sensing observations for oil spill monitoring. Environmental Science and Pollution Research International, 24, 5530-5543.

De Padova, D., De Serio, F., Mossa, M., Armenio, E., 2017. Investigation of the current circulation offshore Taranto by using field measurements and numerical model. In Proceedings of the 2017 IEEE International Instrumentation and Measurement Technology Conference (I2MTC), Turin, Italy, 22–25 May 2017.

De Pascalis, F., Ghezzo, M., Umgiesser, G., De Serio, F., Mossa, M., 2016a. Use of SHYFEM open source hydrodynamic model for time scales analysis in a semi-enclosed basin. Proc. Environmental, Energy, and Structural Monitoring Systems (EESMS), 2016 IEEE Workshop pp. 1-4

De Pascalis, F., Petrizzo, A., Ghezzo, M. Lorenzetti, G., Manfè G., Alabiso G. Zaggia L., 2016b. Estuarine circulation in the Taranto Sea. Environmental Science and Pollution Research, 23(13), 12515-12534

De Serio, F., Mossa, M., 2016. Assessment of hydrodynamics, biochemical parameters and eddy diffusivity in a semi-enclosed Ionian basin. J. Deep-Sea Res. II, 133, 176–185.

De Serio, F., Mossa, M., 2018. Meteo and Hydrodynamic Measurements to Detect Physical Processes in Confined Shallow Seas. Sensors, 18(1), 280.

Di Bernardino, A., De Serio, F., Mossa, M., Pini, A., Leuzzi, G., Monti, P., 2016. Micrometeorological simulations over coastal area using CALMET data. Proc. IEEE EESMS 2016: 180-185; ISBN: 978-1-5090-2369-1

Dronkers, J., Zimmerman, J.T.F., 1982. Some principles of mixing in tidal lagoons. In: Oceanologica Acta Procedings of

the International Symposium on Coastal Lagoons, Bordeaux, France, 1981, 107–117.

Ferrarin, C., Bajo, M., Bellafiore, D., Cucco A., De Pascalis F., Ghezzo M., Umgiesser G., 2014. Toward homogenization of Mediterranean lagoons and their loss of hydrodiversity. Geophysical Research Letters 41(16), 5935-5941.

Gaeta, M.G., Samaras, A.G., Federico I., Archetti, R., Maicu, F., Lorenzetti, G., 2016. A coupled wave–3-D hydrodynamics model of the Taranto Sea (Italy): a multiple-nesting approach. Nat. Hazards Earth Syst. Sci., 16, 2071–2083.

Gariazzo, C., Papaleo, V., Pelliccioni, A., Calori, G., Radice, P., Tinarelli, G., 2007. 'Application of a Lagrangian particle model to assess the impact of harbour, industrial and urban activities on air quality in the Taranto area, Italy. Atmospheric Environment, 41(30), 6432-6444.

Geuzaine, C., Remacle, J.F., 2009. Gmsh: a three-dimensional finite element mesh generator with built-in pre- and post-processing facilities. Int. J. Numer. Meth. Engng, 0, 1–24.

Ghezzo, M.; Guerzoni, S.; Cucco, A., Umgiesser, G., 2010. Changes in Venice lagoon dynamics due to construction of mobile barriers. Coastal Engineering, 57(7), 694–708.

Ghezzo, M., De Pascalis, F., Umgiesser, G., Zemlys, P., Sigovini, M., Marcos, C., Pérez-Ruzafa, A., 2015. Connectivity in three European coastal lagoons. Estuaries and coasts, 38(5), 1764-1781, Springer US.

Guélorget, O., Perthuisot, J., 1992. Paralic ecosystems. Biological organization and functioning. Vie Milieu 42, 215–251

Jordi, A., Ferrer, M. I., Vizoso, G., Orfila, A., Basterretxea, G., Casas, B., Alvarez, A., Roig, D., Garau, B., Martinez, M., Fernandez, V., Fornes, A., Ruiz, M., Fornos, J. J., Balaguer, P., Duarte, C. M., Rodriguez, I., Alvarez, E., Onken, R., Orfila, P., Tintore, J., 2006. Scientific management of Mediterranean coastal zone: A hybrid ocean forecasting system for oil spill and search and rescue operations. Mar. Pollut. Bull., 53, 361–368.

Kjerfve, B., Magill, K.E., 1989. Geographic and Hydrodynamic Characteristics of Shallow Coastal Lagoons. Marine Geology, 88, 187-199.

Lisco, S., Corselli, C., De Giosa, F., Mastronuzzi, G., Moretti, M., Siniscalchi, A., Marchese, F., Bracchi, V., Tessarolo, C., Tursi, A., 2016. Geology of Mar Piccolo, Taranto (southern Italy): the physical basis for remediation of a polluted marine area, Journal of Maps, 12(1), 173-180.

Luketina, D., 1998. Simple Tidal Prism Models Revisited. Estuarine Coastal and Shelf Science, 46, 77–84.

Pelliccioni, A., P. Monti and G. Leuzzi, 2015. An alternative wind profile formulation for urban areas in neutral conditions. Environmental Fluid Mechanics, 15, 135-146.

Petenko, I., Mastrantonio, G., Viola, A., Argentini, S., Coniglio, L., Monti, P., Leuzzi, G., 2011. 'Local circulation diurnal patterns and their relationship with large-scale flows in a coastal area of the Tyrrhenian Sea. Boundary-Layer Meteorology, 139(2), 353-366.

Prandle, D., 1984. A modelling study of the mixing of 137Cs in the seas of the European Continental Shelf. Philosophical Transaction of the Royal Society of London, 310, 407–436.

Samaras, A. G. Gaeta, MG, Miquel, A.M. Renata Archetti, R., 2016. High-resolution wave and hydrodynamics modelling in coastal areas: operational applications for coastal planning, decision support and assessment. Natural Hazards and Earth System Sciences, 16(6), 1499-1518.

Sanford, P. L., Boicourt W. C. S.R., 1992. Model for Estimating Tidal Flushing of Small Embayments. Journal of Waterway, Port, Coastal, and Ocean Engineering, 118 (6), 635-654.

Scire, J.S., Robe F.R., Fernau M.E., Yamartino R.J., 2000. 'A User`s guide for the CALMET meteorological model (version 5.0)', Concord, MA, USA: Earth-Tech Inc.

Takeoka, H., 1984. Fundamental concepts of exchange and transport time scales in a coastal sea. Continental Shelf Research, 3(3), 311–326.

Trotta, F., Pinardi, N., Fenu, E. GrandiA, Lyubartsev, V., 2017. Multi-nest high-resolution model of submesoscale circulation features in the Gulf of Taranto. Ocean Dynamics, 67, 1609 – 1625.

Umgiesser, G., Canu, D.M., Cucco, A., Solidoro, C., 2004. A finite element model for the Venice Lagoon. Development, setup, calibration and validation. J Mar Syst, 51, 123–145.

Umgiesser, G., C. Ferrarin, A. Cucco, F. De Pascalis, D. Bellafiore, Ghezzo, M., Bajo, M., 2014.Comparative hydrodynamics of 10 Mediterranean lagoons by means of numerical modeling. J. Geophys. Res. Oceans, 119, 2212–2226, doi: 10.1002/2013JC009512.

Valerio, G., Cantelli, A., Monti, P., Leuzzi, G., 2017. A modeling approach to identify the effective forcing exerted by wind on a prealpine lake surrounded by a complex topography. Water Resources Research, 53, 4036-4052.

Wang, C. F., Hsu, M. H., Kuo, Y. A., 2004. Residence time of the Danshuei River estuary, Taiwan Estuarine. Coastal and Shelf Science, 60, 381- 393.

Wróbel-Niedźwiecka, I., Drozdowska, V., Piskozub, J., 2019. Effect of drag coefficient formula choice on wind stress climatology in the North Atlantic and the European Arctic. Oceanologia, 61(3), 291-299

Zannetti, P., 1990. Air pollution modeling: theories, computational methods, and available software. Computational Mechanics Publications, New York.

Zimmuman, J. T. F., 1976. Mixing and flushing of tidal embayments in the western Dutch Wadden Sea, Part II: Analysis of mixing processes. Neth. J. Sea Res., 10, 397 - 439.